Thesis/
Reports
Waggoner,
A.P.

AIRBORNE OBSERVATIONS OF EMISSIONS FROM THE CLEARWATER BIOMASS FIRES

Loop Agreement
University
of
Washington

CLOUD AND AEROSOL RESEARCH GROUP

AIRBORNE OBSERVATIONS OF EMISSIONS FROM THE CLEARWATER BIOMASS FIRES

by

Alan P. Waggoner, Peter V. Hobbs
Dean A. Hegg, J. David Nance
and Ray E. Weiss

UNIVERSITY OF WASHINGTON
DEPARTMENT OF ATMOSPHERIC SCIENCES
SEATTLE, WASHINGTON
98195

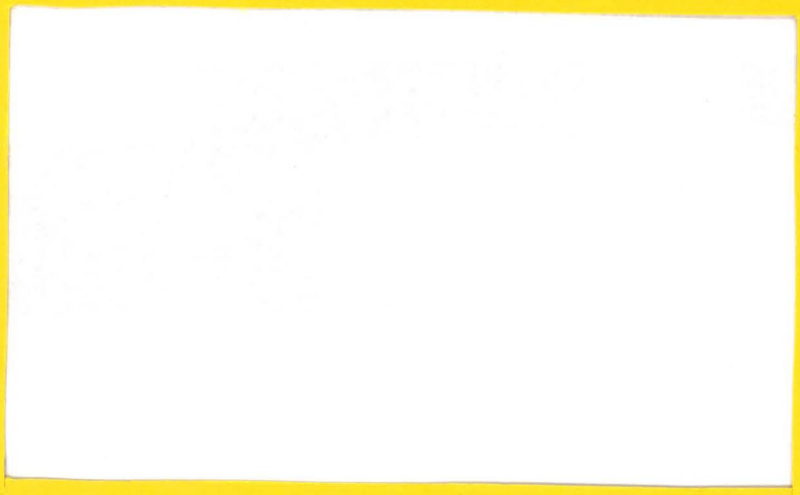

Property of
National FS Library
USDA Forest Service
240 W Prospect Rd
Fort Collins CO 80526

AIRBORNE OBSERVATIONS OF EMISSIONS FROM THE CLEARWATER BIOMASS FIRES

by

Alan P. Waggoner, Peter V. Hobbs
Dean A. Hegg, J. David Nance
and Ray E. Weiss

4 June 1992

This research was supported in part by funds provided by the British Columbia Ministry of Forests, and the Intermountain Research Station, Forest Service, U. S. Department of Agriculture.

Coop Agreement
University
OF
Washington

FINAL REPORT FOR RESEARCH JOINT VENTURE AGMT
#INT-91649-RJVA with
UNIVERSITY OF WASHINGTON
FS contact: Dr. Darold E. Ward
Co-op Contact: Drs Alan P. WAggoner and
Peter V. Hobbs

TABLE OF CONTENTS

	Page
SUMMARY	iii
1. INTRODUCTION	1
2. MEASUREMENT TECHNIQUES	2
3. RESULTS	4
3.1 Concentrations of Gases and Particles in the Smoke Plumes	4
3.2 Emission Factors and Combustion Efficiency	5
3.3 Smoke Optical Properties and Particle Mass Concentrations	9
3.4 Cloud Processing of the Smoke	11
3.5 Particle Size Distributions in the Smoke	11
3.6 Remote and *In Situ* Measurements of Areal Cross Sections of the Smoke Plume and Optical Scattering Coefficient on 15 September	13
4. COMPARISONS WITH SOME OTHER BIOMASS FIRES	16
5. REFERENCES	17
APPENDIX: THE UNIVERSITY OF WASHINGTON'S CONVAIR C-131A RESEARCH AIRCRAFT	A-1

SUMMARY

Airborne measurements were made of the smoke from two prescribed burns of forest slash near Clearwater in Eastern British Columbia, Canada, on 15 and 16 September 1991. Each burn was ~33 hectares in area and the debris consisted of western red cedar, Douglas fir and subalpine fir. We characterize the smoke in terms of the concentrations and emission factors for particle mass (<3.5 μm), and for gaseous CO_2, CO, N_2O, NO_x, CH_4, and various hydrocarbons.

Emission factors from the two fires differed somewhat from each other, and from some of our previous measurements on biomass fires. These differences may be due to the restricted sampling intervals, 45–120 minutes after ignition for the first fire and 15–58 minutes after ignition for the second fire. Compared to previous measurements, the first fire had high emission factors for CH_4 and smoke particle mass and low emissions of N_2O. The second fire had high emissions of N_2O. Both fires had low emissions of NO_x. We also measured the size distribution, mass concentration, and optical properties of particles in the smoke column from the 16 September fire for comparison with similar measurements made on smoke that had passed through a cloud that formed at the top of the smoke column. We found no major effects that can be attributed to cloud processing in terms of enhanced particle removal or reduced visual impact of the smoke. However, there were changes in the particle size distribution that would be expected to enhance light scattering by smoke particles.

The transport and dispersion of smoke from the fire was measured on 15 September, using a downward-looking lidar on the aircraft to measure the cross-sectional areas of the plume, and optical scattering extinction coefficients at several distances downwind of the fire. Between 1 and 1 1/2 hours after ignition, the width of the plume was 6 km at 9 km downwind, 10 km at 18 km downwind, and 11 km at 41 km downwind. The plume cross sections had several regions of high concentration, undoubtly resulting from the pattern and rate of ignition, and were much more complex in shape than a Gaussian plume model would predict.

AIRBORNE OBSERVATIONS OF EMISSIONS FROM THE CLEARWATER BIOMASS FIRES

1. INTRODUCTION

Emissions from biomass burning are an important source of several trace gases in the atmosphere, including carbon dioxide (CO_2), methane (CH_4), hydrocarbons, and oxides of nitrogen (NO and NO_2). Particles in the smoke emitted from biomass burning can have regional impacts on visual air quality, on the scattering and absorption of solar radiation and, perhaps, on human health. Consequently, in recent years, emissions into the atmosphere from biomass burning, and the transport and dispersions of these emissions, have been the subject of increased interest.

Because of the need to provide smoke management guidelines to foresters in the conduct of prescribed burns of residue left from the harvesting of timber, measurements were made of the smoke from two prescribed burns near Clearwater, British Columbia, on 15 and 16 September 1991. On 15 September, we characterized the smoke plume from a fire 31.8 hectares in area, consisting of 49% western red cedar, 22% Douglas fir, and 25% subalpine fir, located at 51.682° N and 120.109° W at a ground elevation of about 1200 meters above mean sea level. On 16 September, we studied the smoke plume from another fire of 33.4 hectares (no fuel inventory available), at a surface elevation of 1350 m MSL, located at 51.823° N, 120.153° W. The results of the two studies are described in this report and are compared to previous measurements of the conversion of biomass to airborne emissions and transport of smoke over distances up to several 100 km made in similar fires in the United States and Canada by the University of Washington Cloud and Aerosol Research Group.

2. MEASUREMENT TECHNIQUES

The airborne measurements were made aboard the University of Washington's Convair C-131A research aircraft using instruments described in Appendix A (Hobbs *et al.*, 1991). The aircraft flew through the rising columns of smoke from the fires, and in and above the spreading downwind smokes plumes. The concentrations of CO_2, CO, O_3, various hydrocarbons and oxides of nitrogen in the smoke were measured with various continuous gas sampling instruments (see Appendix A). During penetrations of the smoke columns, a plastic bag in the aircraft was filled with smoke in about 10 seconds and, during the next few minutes, smoke samples were drawn from this bag into the various measuring instruments. Optical scattering coefficients (σ_{scat}) and optical extinction coefficients (σ_{ext}) were determined using an integrating nephelometer and an optical extinction cell, respectively, sampling ram air. Particle size distributions in the size range that dominates optical extinction (0.1 to 2 μm) and particle mass concentration (0.1 to 10 μm) were measured from bag samples using several instruments described in Appendix A. The mass concentrations of smoke particles, and particle optical absorption coefficients, were determined from samples made by filtering the air through Teflon filters from the plastic sampling bag. Gas samples collected in stainless-steel bottles were analyzed to determine concentrations of carbon monoxide (CO), carbon dioxide (CO_2), methane (CH_4), total non-methane hydrocarbons (TNMHC) and N_2O. These samples were analyzed by R. A. Rasmussen at the Oregon Graduate Institute of Science and Technology (Rasmussen *et al.*, 1980; Rasmussen and Khalil, 1981). The carbonaceous gas concentrations were measured by flame-ionization, gas-chromatography with analytic uncertainties of 0.5%, 5%, 0.3–0.4% and 10% for CO_2, CO, CH_4 and TNMHC, respectively (Rasmussen, personal communication, 1992). N_2O concentration was measured using an electron-capture, gas-chromatographic technique with an analytic uncertainty of <1% (Rasmussen *et al.*, 1980; Rasmussen

and Khalil, 1981). The extent of the smoke from the fire was measured both by flying transversely through the smoke plume at several distances downwind from the fire and obtaining *in situ* measurements with an integrating nephelometer, and by flying above the plume and using a lidar to remotely sense the particles in the plume.

The average degree of asymmetry in particle shape was determined using an electro-optical response (EOR) instrument, which measures the fractional change in the optical scattering coefficient as particles align in response to a pulsed electrical field (Kaputsin, *et al.*, 1980). The response from the EOR is ~ 20–30% for fresh soot from oil fires (Weiss *et al.*, 1992), and 0 to 10% for smoke from biomass fires (variations are related to relative humidity, combustion efficiency, age of smoke, etc.).

Particle mass concentrations were measured by sampling from the aircraft bag to collect particles on 37 mm Teflon filters. The filters were subsequently weighed using a Cahn model 21 electro-balance with 1 μg resolution. All filters were pre-weighed prior to sampling; three filters were used as blanks (+3 μg average weight gain, likely caused by transfer of material from the filter holder to the filter). The filters were also used to measure optical absorption from the decrease in diffuse optical transmission (Weiss *et al.*, 1979).

Simultaneous paired filter samples, one with a cyclone to exclude particles larger than 3.5 μm diameter and one without a cyclone, were taken on 15 September. However, flow transducers on the line containing the cyclone failed and therefore this data could not be used. Filter samples on 16 September were taken without the cyclone. Even in the absence of a cyclone, we believe that only particles with a diameter <3.5 μm were collected. This is because particle size distributions for biomass smoke measured from our aircraft in this and in other projects show

negligible particle volume or mass for particles with diameters between ~1.2 and ~7 μm (for example see figure 4 in this report). Thus, a filter sample with any upper size cut-off between ~1.2 and ~7 μm would measure essentially the same particle mass concentration. In our past studies, similar smoke particle mass concentrations have always been measured, with and without the 3.5 μm cut point cyclone. This is probably due to the sampling inlet system on the aircraft excluding particles with a diameter greater than an undetermined value in the range, 1.2 - 7 μm. Thus, we believe that the particle mass concentration data obtained in this field study without a cyclone are equivalent to our earlier data taken with a 3.5 μm cut diameter cyclone.

3. RESULTS

3.1 Concentrations of Gases and Particles in the Smoke Plumes

In both fires, several "grab-bag" samples of air were collected and analyzed from the rising columns of smoke, in the horizontally spreading smoke plume, and in the background air outside of the smoke plumes. Table 1 lists the gas concentrations in the smoke and in the background air for all species except NO_X. NO_X concentrations were measured using real time instrumentation, and are reported as the difference between smoke-laden air and adjacent background air.

The CO_2 concentrations in the smoke were elevated by up to 80 ppm above the background concentrations of about 352 ppm. Measured concentrations of N_2O in the smoke were elevated above background concentrations (~340 ppb) by up to 2 ppb on 15 September and by up to 30 ppb on 16 September. Measured concentrations of CH_4 in the smoke were elevated by up to 1,200 ppb above a background concentration of ~1,800 ppb. CO, NO_X, non-methane hydrocarbons (Non-methane hydrocarbons consist of C_2 to C_{10} plus unidentified hydrocarbons as

Table 1: Mass mixing ratios of gases and particles in the plumes from the two prescribed fires in British Columbia on 15 and 16 September 1991.

Date (1991)	Sample Type*	Altitude (km)	Time (hhmm PDT)	Particle Mass ($\mu g\ m^{-3}$)	CO (ppb)	CO_2 (ppm)	CH_4 (ppb)	TNMHC (ppbC)	N_2O (ppb)	NO_x† (ppb)
15 Sept	column	2.3	1516	633	4446	390	2317	966	343.6	ND#
	column	2.3	1526	1579	10196	431	3025	1916	341.9	ND
	plume (15)	2.9	1541	654	2481	376	2080	504	341.6	3.65
	plume (40)	2.9	1615	157	171	354	1797	191	342.6	ND
	column	2.2	1627	279	2362	378	2062	518	342.8	4.13
	background	2.9	1711		82	353	1784	55	ND	0
	background	2.9	1722	26	80	354	1778	57	341.8	0
16 Sept	column	1.7	1434	337	2744	412	2041	691	343.6	24.3
	column	1.7	1442	728	4693	421	2299	1135	366.2	25.4
	post-cloud	2.8	1517	349	2229	392	2018	468	362.0	16.0
	background	2.3	1537		89	351	1795	101	ND	0
	background	2.3	1545	34	89	351	1787	52	338.6	0

* Sample types labelled "column" were collected in the ascending column of smoke above the fire. Those labelled "plume (x)" were collected in the stabilized plume ~x km downwind of the fire. The smoke sample labelled "post-cloud" had just passed through a cumulus cloud that was capping the smoke column. Samples labelled "background" were collected in background air located upwind of the fire.

† Plume minus background concentrations.

ND = no data.

reported to us by R. A. Rasmussen. The concentration of unidentified species was ~25% of total NMHC.), and particle mass concentrations were all elevated in the smoke by a factor of ten or more above background concentrations in both fires.

The measured concentrations of CO, particles and CH_4 in the column smoke were higher on 15 September than on 16 September. On 15 September, the concentrations of NO_x in the column smoke were lower than on 16 September. This was probably due to differences in the times at which the two fires were sampled. (On 15 September, the column smoke was sampled five times, between 45 to 116 minutes after ignition. On 16 September, the column was sampled three times between 15 to 58 minutes after ignition.)

Table 1 also lists the measured particle mass concentrations in the two fires. As noted in Section 3.1, these measurements were made without a cyclone, but are considered by us equivalent to our earlier measurements of particles with diameters <3.5 μm. Measurements in other biomass fires have yielded similar particle mass concentrations to those listed in Table 1 (Radke *et al.*, 1991).

3.2 Emission Factors and Combustion Efficiency

The emission factor of a chemical species is defined as the mass of the species emitted into the air per unit mass of wood burned. Emissions factors can be calculated from measured concentrations (above ambient) of all the airborne carbon containing species in the smoke plume (Ward *et al.*, 1982; Radke *et al.*, 1988).

The combustion efficiency (CE) of a fire is defined as the percentage of carbon in the emissions that is in the form of CO_2. Forest fires generally evolve in two stages: flaming combustion and smoldering combustion (Ward, 1990; Radke, *et al.*, 1991; Laursen, *et al.*, 1992). Flaming combustion occurs early in the life cycle of a fire, with

vigorous air motions driven by high rate of thermal energy release. This generates strong turbulence that brings plentiful oxygen into contact with the fuel and combustible gases to produce rapid burning, high combustion efficiency, and low emissions of CO, CH_4, total non-methane hydrocarbons (TNMHC) and smoke particles (Ward, 1990; Laursen, *et al.*, 1992). In the smoldering stage of combustion, the rate of heat release is much lower, and turbulence is reduced to the point where the burn rate is limited by the diffusion of oxygen to the burning embers (Ward, 1990; Laursen, *et al.*, 1992). During smoldering combustion, the reduced availability of oxygen lowers the combustion efficiency so that the emissions of CO, CH_4 and condensed hydrocarbons are increased (Ward, 1990; Laursen, *et al.*, 1992). Graphitic carbon (or soot) appears to form a higher fraction of the particulate matter in smoke during flaming combustion than it does during smoldering combustion (Radke *et al.*, 1991). The probable source of this soot is the combustion of gaseous pyrolysis emissions in a fuel-rich environment, where combustion preferentially removes hydrogen from the gas molecules, leaving a sooty residue (Glassman, 1977; Ward and Hardy, 1991).

Ground-based measurements of prescribed burns, primarily of forest slash, indicate that by far the most important form of carbon in the emissions is CO_2 (Ward and Hardy, 1991). However, the fraction of the carbon in the fuel that is converted into CO_2 varies depending on the stage of combustion (flaming or smoldering). The remaining carbon is partitioned between CO (~9.5%), smoke particles (~1.5%), CH_4 (~0.5%) and other non-methane hydrocarbons (~0.5%) (Ward and Hardy, 1991). The transition from flaming to smoldering combustion can lead to distinctive characteristics in the emissions from biomass burns with limited supplies of fuel. Flaming combustion tends to be efficient producing relatively high quantities of CO_2 (i.e. high CE) and relatively low quantities of CO and hydrocarbons. During

smoldering combustion, more CO and hydrocarbons are produced at the expense of CO_2. These changes are reflected in our measurements, shown in Table 2.

The time of our first smoke sample on 15 September was 45 minutes after fire ignition. At this time, the smoke plume had risen to an altitude of ~3 km, but the column of smoke was showing signs of collapse due to substantially reduced heat output from the fire. The four smoke samples obtained during this flight were characteristic of smoldering combustion, with a mean CE of (86 ± 2)%.

In the 16 September burn, we collected two samples of smoke in the vigorously ascending column of smoke produced by flaming combustion, and one sample in smoke that has passed through a water cloud capping the smoke column. The mean CE was (93 ± 2)%, which is significantly higher than the CE measured the previous day in the smoke from smoldering combustion. Also, the mean emission factors for particles, CO, CH_4 and TNMHC on 16 September were about a factor of two smaller than those on 15 September.

Table 2 lists the derived combustion efficiencies for various species from the two fires. The emission factors for particles, CO, CH_4 and TNMHC versus CE are shown in Fig. 1 (particles and CO) and Fig. 2 (CH_4 and TNMHC) for all eight smoke samples collected in the two fires. Also plotted in Figs. 1 and 2, are regression relations (derived from ground-based sampling by Ward and Hardy, 1991) that relate emission factors for particles less than 2.5 μm in diameter, CO, and CH_4 to CE. There is good agreement between our measurements of emission factors for CO, and for particles <2.5 μm in diameter, versus CE and that predicted by Ward and Hardy's relations. Our aircraft measurements and Ward's ground measurements of

Table 2: Emission factors* and combustion efficiencies (CE)† computed from the data listed in Table 1#.

Date (1991)	Sample Type**	Time (hhmm PDT)	Particle Mass ($g\ kg^{-1}$)	CO_2 ($g\ kg^{-1}$)	CO ($g\ kg^{-1}$)	CH_4 ($g\ kg^{-1}$)	TNMHC ($gC\ kg^{-1}$)	N_2O ($g\ kg^{-1}$)	NO_x ($g\ kg^{-1}$)	CE (%)
15 Sept	column	1516	13.3	1551	118	8.3	10.5	0.08		85
	column	1526	15.9	1532	127	8.9	10.0	0.00		84
	plume (15)	1541	22.5	1562	106	7.6	8.5		0.26	86
	column	1627	8.6	1608	95	6.7	8.3	0.07	0.27	88
	arithmetic mean		15.1	1563	112	7.9	9.3	0.04	0.27	86
	± standard deviation		± 5.8	± 32	± 14	± 1.0	± 1.1	± 0.04	± 0.01	± 2
16 Sept	column	1434	4.4	1715	48	2.6	4.7	0.07	0.56	94
	column	1442	8.5	1660	69	4.4	6.9	0.61	0.53	91
	post-cloud	1517	6.7	1696	56	3.4	4.4	0.88	0.64	93
	arithmetic mean		6.5	1691	58	3.5	5.3	0.52	0.58	93
	± standard deviation		± 2.1	± 28	± 11	± 0.9	± 1.3	± 0.41	± 0.06	± 2
All samples from both fires	arithmetic mean		11.4	1618	89	6.0	7.6	0.25	0.45	89
	± standard deviation		± 6.2	± 73	± 31	± 2.5	± 2.4	± 0.35	± 0.18	± 4

* Units are grams of compound produced per kilogram of fuel burned for particles, CO_2, CO, CH_4, N_2O, and NO_x, and grams of carbon per kilogram of fuel for TNMHC.

† CE is the combustion efficiency (defined as the percentage of the total carbon in the emissions that is in the form of CO_2).

The sample collected at 1615 PDT on 15 September, 1991 (see Table 1) was excluded due to insufficient plume minus background CO_2 signal.

** See first footnote to Table 1.

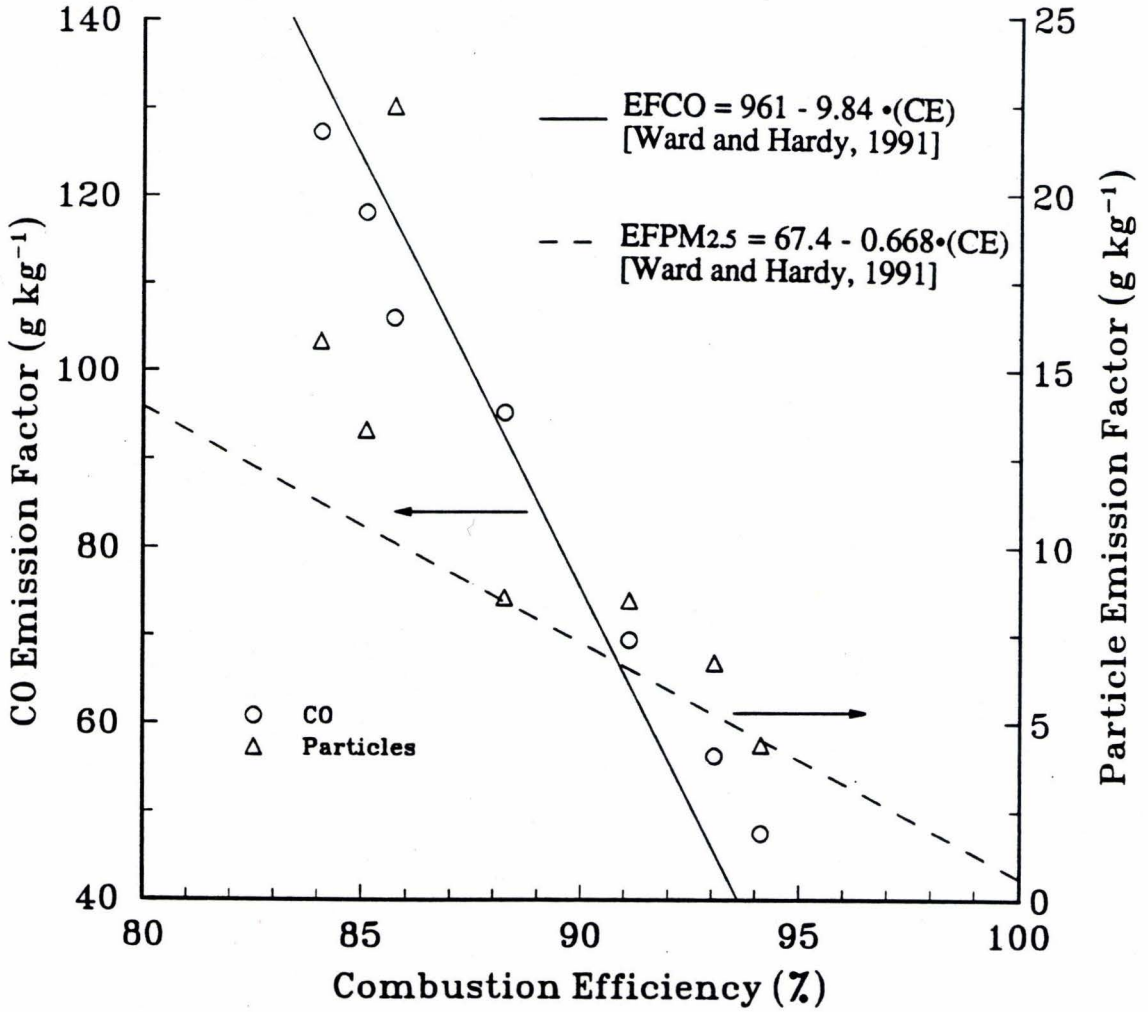

Figure 1. CO and particle <3.5 μm emission factors versus combustion efficiency for the combined aircraft data from the Clearwater fires on 15 and 16 September 1991. The data are compared to the regression lines reported by Ward and Hardy (1991) for CO and for particle mass, <2.5 μm in diameter, based on measurements near ground level at several other prescribed fires.

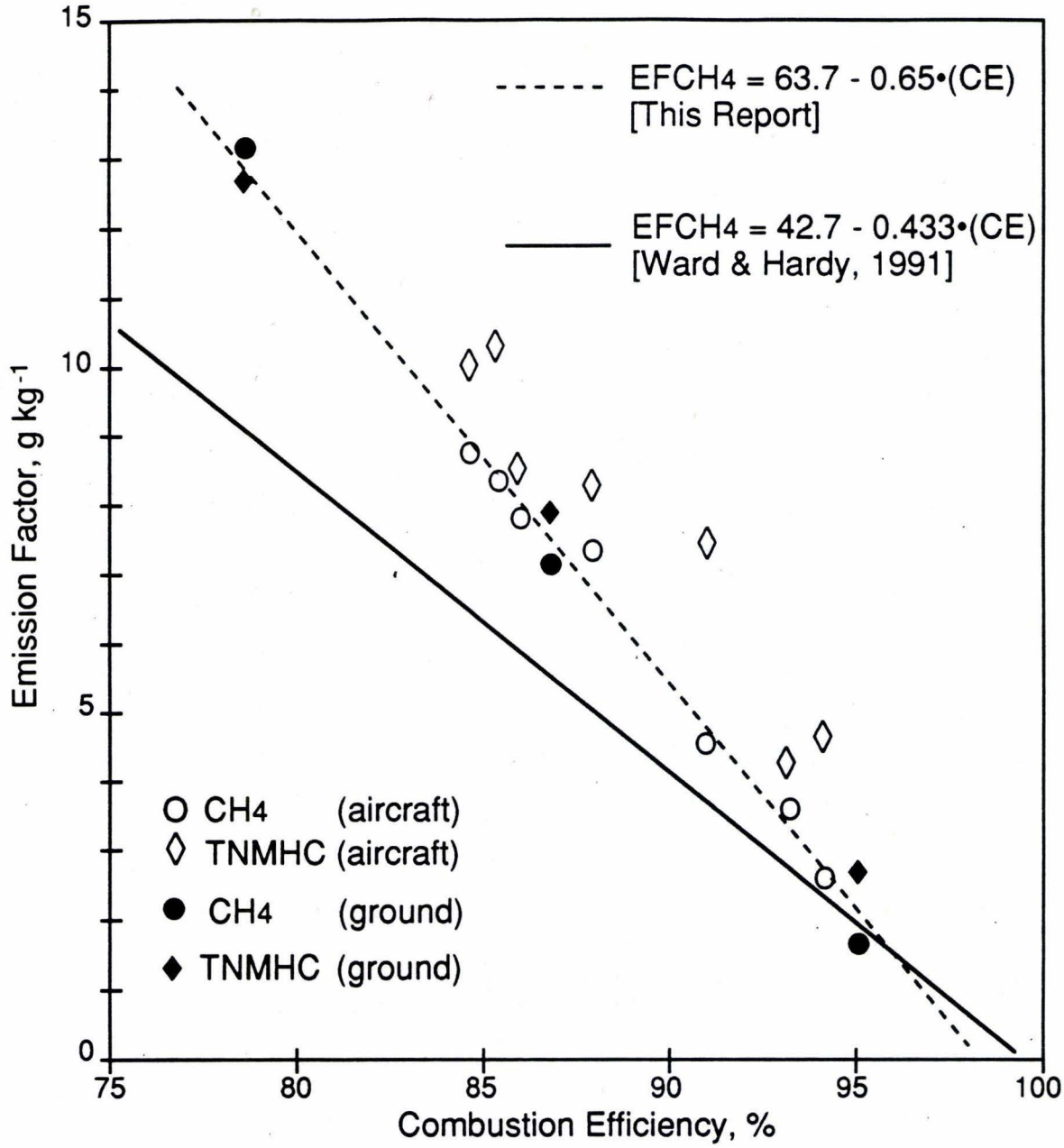

Figure 2. Methane and total non-methane hydrocarbon emission factors versus combustion efficiency for the Clearwater fires. The open symbols are from analysis of aircraft samples of column smoke from both the 15 and 16 September fires. The darkened symbols are from ground based measurements on the 15 September fire only, reported to us by Ward (personal communication, 1992). The combined data set is compared to the regression line reported by Ward and Hardy and the best-line fit to our data. Note the close agreement between the aircraft and ground sampling.

the Clearwater CH_4 emission factor versus CE are in close agreement, but somewhat higher than that previously published by Ward and Hardy (1991).

The CH_4 emission factors for both fires as a function of combustion efficiency, which are shown in Fig. 2, are large in comparison to ten other fires we have studied over the past six years (see Section 4). Also, the measurements for the two Clearwater fires lie above the regression line of Ward and Hardy (1991). The mean CH_4 emission factor computed from data collected at the ten previous fires studied by us is 3.2 g kg^{-1} (Radke *et al.*, 1991). This is lower than the mean CH_4 emission factor for the Clearwater fire of 16 September (3.5 g kg^{-1}). However, as noted previously, we sampled this fire during flaming combustion, for which CH_4 emissions are expected to be low. The mean CH_4 emission factor computed from the samples collected on 15 September (7.9 g kg^{-1}), which was sampled mainly during smoldering combustion, is the largest we have ever measured for any biomass fire (Radke *et al.*, 1991). When the samples collected at both Clearwater fires are combined, the mean emission factors for CO_2 and CO are within 8% of the average value for the ten biomass fires discussed by Radke *et al.* (1991), but the mean CH_4 emission factor for the two Clearwater fires is almost twice as great as the average for the ten fires.

The N_2O emission factors in Table 2 indicate that it was produced in greater quantities by the fire of 16 September than by the 15 September fire. This is tentatively confirmed by the results for NO_x which, in conjunction with the N_2O data, shows that substantially more gaseous nitrogen species were released on 16 September than on 15 September, 1991. This is consistent with laboratory studies, which have shown that emission factors for N_2O and NO_x are higher during flaming combustion than during smoldering combustion (e.g. Crutzen and Andreae, 1990). When averaged over both fires, the N_2O emission factor of 0.25 g kg^{-1} of fuel is

consistent with the average value obtained from our studies of eight previous fires (0.23 g per kg of fuel; Radke *et al.*, 1991). However, for the two Clearwater fires, the mean NO_x emission factor of 0.45 grams per kilogram of fuel burned is strikingly low in comparison with our previous results (1.3 g kg^{-1} of fuel; Radke *et al.*, 1990). The three fires with the highest NO_x emission factors we have measured burned near very large urban areas in southern California, where NO_x pollutant deposition into the fuel bed apparently enhanced the NO_x emissions during fuel combustion (Hegg *et al.*, 1987). Even the fire that we studied previously with the lowest emission factor fire ("Battersby"; 0.35 g kg^{-1}; Radke, *et al.*, 1991) had an NO_x emission factor that was twice the value that was measured on 16 September (Table 2). The nitrogen content of the fuel may have been lower in rural British Columbia, Canada, than at the urban-affected California sites (Evans *et al.*, 1977; Clements and McMahon, 1980; Logan, 1983).

3.3 Smoke Optical Properties and Particle Mass Concentrations

Airborne measurements were obtained of the optical properties and particle mass concentrations of the smoke from the two fires in British Columbia on 15 and 16 September 1991. Real time optical instruments, operating off a common inlet port, included an integrating nephelometer to measure the light-scattering coefficient (σ_{scat}), and a 6.4 meter length optical extinction cell to measure the optical extinction coefficient (σ_{ext}), which is equal to the sum of the light-scattering (σ_{scat}) and optical absorption (σ_{abs}) coefficients. The optical extinction coefficient is a measure of the visibility reducing potential of the smoke, and the optical absorption coefficient is a measure of the concentration of graphitic carbon (or soot) in the smoke particles. Optical extinction is due primarily to particles smaller than 2 μm diameter (Waggoner and Weiss, 1980).

Particle mass concentrations were measured using filters that sampled smoke from the "grab bag". The "grab bag" fills in about 10 seconds, or about 800 meters of flight under normal sampling conditions. This sample distance is longer than the usual diameter of the smoke column so the sample contains column smoke and some surrounding clean air. The data system that recorded the nephelometer and extinction cell data versus time also recorded the opening and closing times of the "grab bag" inlet valve. We use these two times plus the nephelometer measure of scattering coefficient versus time to correct for the fraction of clean air that is sampled with column smoke. For example, if the column is sampled for 5 seconds and clean air for 5 seconds, the measured particle mass concentration determined from "grab bag" samples would be increased by a factor of 2 to correct for the bag containing a mixture of equal parts smoke and clean air.

Tables 3 and 4 list the following data as a function of time for each of the two Clearwater fires:

- Mass concentration of particles with diameter < 3.5 μm
- Concentration of particulate graphitic carbon
- Scattering and absorption coefficients per unit mass of particles ($\sigma_{scat}/\rho_{part}$ and σ_{abs}/ρ_{part}, respectively, where ρ_{part} is the mass of particles per unit volume of air)
- Particle single-scattering albedo, $\omega_o \left[\omega_o = \frac{\sigma_{scat}}{\sigma_{scat} + \sigma_{abs}} = \frac{\sigma_{scat}}{\sigma_{ext}}\right]$
- Electro-optical response (EOR).

On 15 September, the single-scattering albedo in the smoke column was high (>0.9), which is typical of measurements from the later stages of fuel limited biomass combustion (Radke *et al.*, 1991). From the measured values of the single-scattering albedo, the percentage of the particle mass that was soot was deduced to be less than 5%. The values of $\sigma_{scat}/\rho_{part}$ and σ_{abs}/ρ_{part} were 4.5 and 0.4 $m^2\ g^{-1}$,

Table 3. Particle mass concentration (ρ_{part} in μg per m^3 of air), soot concentration (in terms of equivalent mass of graphitic carbon in μg per m^3 of air), particle absorption coefficient (σ_{abs}), and the scattering and absoption efficiencies (σ_{scat}/ρ_{par} and σ_{abs}/ρ_{part}) measured in the smoke from two prescribed burns in British Columbia. Data has a probable upper particle size cut at ~3.5 μm due to the sampling system characteristics.

Date (1991)	Filter #	Time (PDT)	Smoke Type†	ρ_{part} ($\mu g\ m^{-3}$)	Soot, concentration $\mu g\ m^{-3}$	σ_{abs} (units of $10^{-4} m^{-1}$)	$\frac{\sigma_{scat}}{\rho_{part}}$ ($m^2 g^{-1}$)	$\frac{\sigma_{abs}}{\rho_{part}}$ ($m^2 g^{-1}$)
15 September Ignition @14:31 PDT	2	1515	old column	633	35	3.45	–	0.545
	4	1525	old column	1579	71	7.11	–	0.450
	6	1541	old column	654	26	2.63	–	0.402
	8	1615	old column	157	2	0.16	4.1	0.104
	10	1627	old column	279	2	1.24	5.1	0.445
	12	1711-1727	ambient	26	1	0.08	-	0.330
16 September Ignition @14:19 PDT	13	1434	early column	337	24	2.37	4.3	0.703
	14	1442	early column	728	49	4.92	4.2	0.676
	15	1453	cloud base	389	41	4.06	5.1	1.040
	16	1517	post-cloud	349	27	2.65	4.1	0.759
	17	1537-1544	ambient	34	1	0.05	-	0.150

†"old column" means the fire began more than 1 hour prior to sampling the column.
"ambient" means samples in air not contaminated with smoke.
"early column" means column smoke was sampled within 30 minutes after ignition.
"cloud base" means column samples from just below cloud base.
"post-cloud" means smoke was sampled just after it passed through the cap cloud.

Table 4. Particle single-scattering albedo and electro-optical response (EOR) for smoke from two prescribed burns in British Columbia on 15 and 16 September 1991.

Date (1991)	Time (PDT)	Smoke Type, Location†	Single-Scattering Albedo ($\omega_o = \sigma_{scat}/\sigma_{ext}$)	EOR (%)‡
15 September Ignition @ 1431 PDT	1606	old column	0.94	BDL
	1612	old column	0.99	BDL
	1615*	old column	0.99	BDL
	1616	old column	0.99	BDL
	1619	old column	0.98	BDL
	1627	old column	0.95	BDL
16 September Ignition @ 1419 PDT	1428	early column	0.67	0.06
	1429	early column	0.66	0.04
	1434*	early column	0.80	0.02
	1442*	early column	0.79	0.02
	1445	early column	0.79	0.01
	1453*	cloud base	0.82	BDL
	1503	cloud base	0.86	BDL
	1507	cloud base	0.87	BDL
	1516*	post-cloud	0.87	BDL
	1523	post-cloud	0.92	BDL
	1529	post-cloud	0.95	BDL

* Times have corresponding filter data for particle mass concentration and optical absorption as listed Table 3.

†"old column" means the fire began more than 1 hour prior to sampling the column.
"early column" means column smoke was sampled within 30 minutes after ignition.
"cloud base" means column samples from just below cloud base.
"post-cloud" means smoke was sampled just after it passed through the cap cloud.

‡"BDL" is below detection limit.

respectively. The EOR instrument showed zero response for all of the measurements in the column of smoke on 15 September. This indicates that the smoke was predominantly spherical particles (probably produced by the high relative humidity).

3.4 Cloud Processing of the Smoke

In the 16 September fire we measured the light-scattering coefficient and the particle mass concentration in the ascending column of smoke, just below cloud base, and after the smoke had passed through a cap cloud that formed at the top of the smoke column (See Fig. 3). At these three locations, the ratio of the light-scattering coefficient to the particle mass concentration (ρ_{part}) was the same to within ±25% (Table 4). In the ascending column of smoke the single-scattering albedo was ~0.7, at cloud base it was 0.85, and in the smoke exiting the cap cloud it was 0.9. In the ascending column of smoke, where the single-scattering albedo was lowest (implying the highest fraction of soot in the smoke), the EOR value was about 6%. This indicates that there was some aggregation of the particles, although the aggregation was small compared to that measured by Weiss, *et al.* (1992) in fresh smoke from the 1991 Kuwait oil fires, which produced an EOR value of 40%.

The effects of cloud processing on particle size distribution in the smoke are discussed in the following sub-section.

3.5 Particle Size Distributions in the Smoke

On 16 September, particle size distributions were measured in the ascending column of smoke and after the smoke had passed through the cap cloud (see Fig. 3). The results are shown in Fig. 4, where particle number and volume concentrations

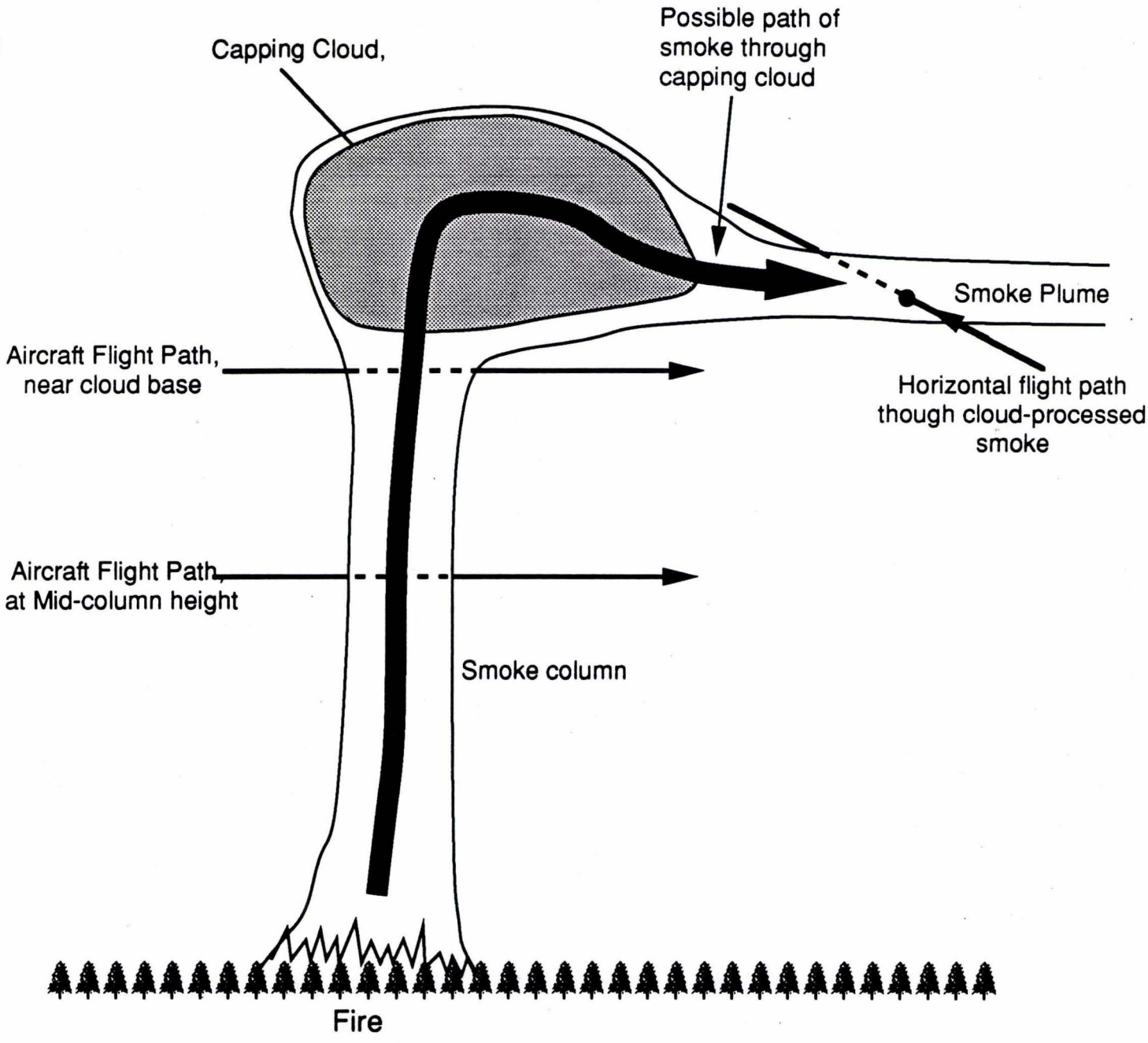
Capping Cloud,
Possible path of smoke through capping cloud
Smoke Plume
Aircraft Flight Path, near cloud base
Horizontal flight path though cloud-processed smoke
Aircraft Flight Path, at Mid-column height
Smoke column
Fire

Figure 3. Aircraft flight paths through the smoke at mid-column height, near cloud base, and through smoke processed by the capping cloud on 16 September 1991.

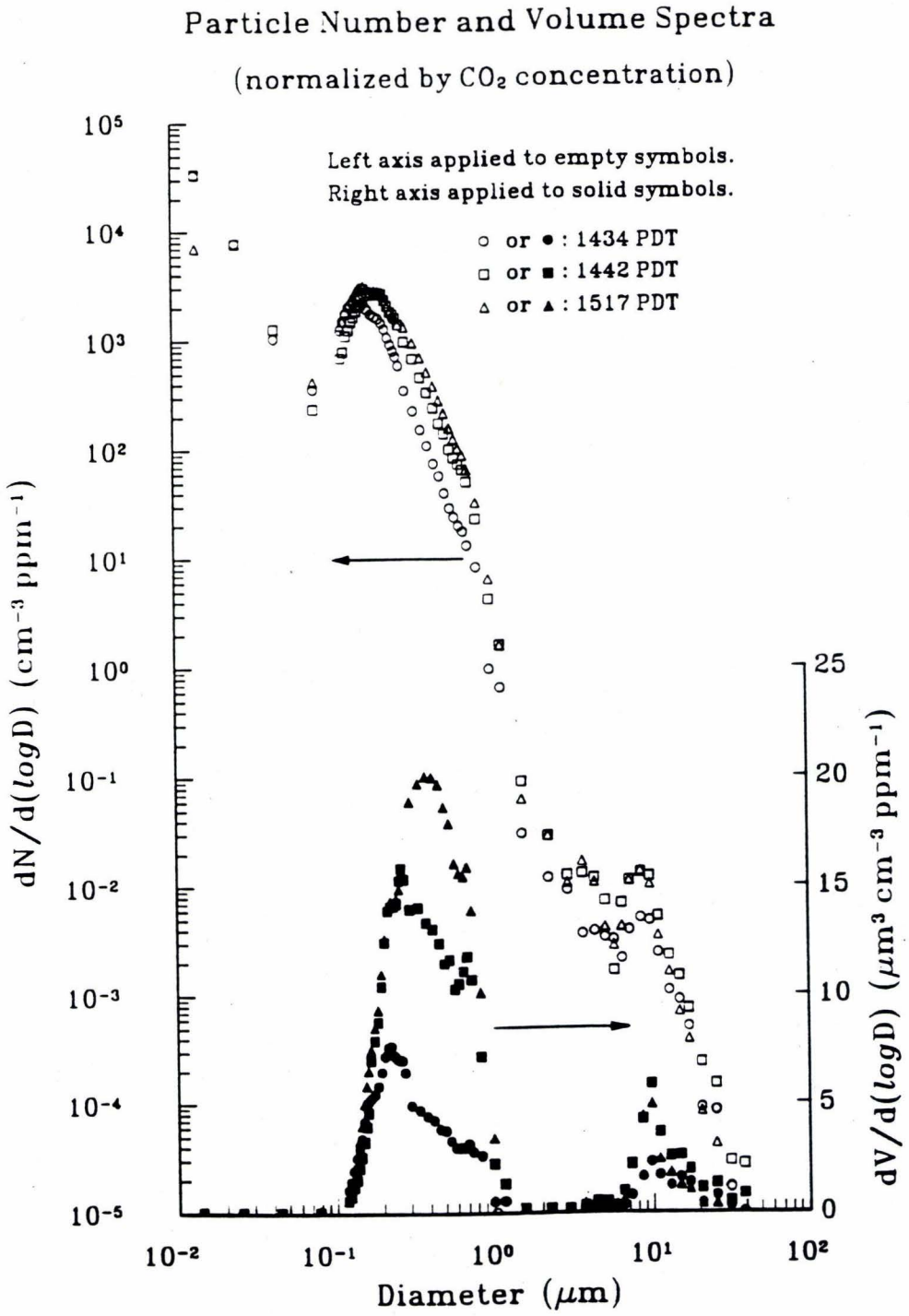
Particle Number and Volume Spectra
(normalized by CO_2 concentration)
Left axis applied to empty symbols.
Right axis applied to solid symbols.
○ or ● : 1434 PDT
□ or ■ : 1442 PDT
△ or ▲ : 1517 PDT
dN/d(logD) (cm^{-3} ppm^{-1})
dV/d(logD) (μm^3 cm^{-3} ppm^{-1})
Diameter (μm)

Figure 4. Particle number (empty symbols) and volume (solid symbols) size spectra for three samples collected in the smoke plume from the Clearwater 2 fire of 16 September, 1991. The samples collected at 1434 and 1442 PDT (represented by circles and squares, respectively) were taken in the vigorously ascending column of smoke below cloud base at an altitude of ~2.0 km. The sample collected at 1517 PDT (represented by triangles) was taken at an altitude of ~3.0 km after the smoke had passed through a water cloud that capped the smoke column (see Figure 4). All spectra have been normalized by the above-background concentration of CO_2.

have been normalized to a constant particle mass concentration in order to correct for dilution effects. The concentrations of particles in the size range 0.2 – 0.8 μm diameter increase with time. In the case of the particle size distribution measured at 1517 PDT, this increase could have been due to cloud processing or to a change in the character of the emitted smoke. There was an increase in particle mass concentration for the particle size where $\sigma_{scat}/\rho_{part}$ reaches a peak value at about 0.6 μm. It might be expected that this increase in relative particle concentration near 0.6 μm would increase the value of $\sigma_{scat}/\rho_{part}$. However, as noted in the previous paragraph, there was no significant difference in the optical scattering properties for the smoke particles sampled before and after cloud processing. Perhaps the change in particle scattering to mass was small enough to be masked by measurement uncertainties or other fluctuations.

As we have seen above, the visual impact of smoke, in terms of the ratio of the optical scattering coefficient to the particle mass concentration ($\sigma_{scat}/\rho_{part}$), appeared to be unchanged to within ±25% after passage of the smoke through the cap cloud. To reduce the optical extinction efficiency of smoke particles, particles with size range in the 0.2 to 2 μm diameter region must be removed from the smoke or transferred to larger particle sizes. The most effective method for the natural removal of this size fraction is to incorporate them into cloud droplets (as cloud condensation nuclei) then for these drops to be removed by precipitation. Scavenging of particles by this process should be most effective for large, precipitating clouds, rather than the small cap cloud that we investigated on 16 September In view of the potential importance of clouds in reducing the opacity of visual plumes and the density of haze from the burning of forest refuse, attempts should be made to obtain data on the interactions of smoke plumes with clouds.

3.6 Remote and *In Situ* Measurements of Areal Cross Sections of the Smoke Plume and Optical Scattering Coefficient on 15 September

A lidar (the optical equivalent of a radar, but for visible and near IR wavelengths) on the University of Washington's Convair C-131A aircraft was used to determine the cross-sectional areas of the smoke plume at various downwind distances from the Clearwater fire on 15 September. The downward-pointing lidar transmits a pulse of light containing two wavelengths, 0.532 and 1.064 μm, of duration ~10^{-8} seconds. Light scattered back toward the lidar by air molecules (Rayleigh scattering) and by particles (Mie scattering) is collected by a 14" diameter telescope and focused onto two single wavelength light detectors. The intensity of the light returned to the lidar versus the time taken for each pulse to return to the lidar is related to the concentration of air molecules and of smoke particles as a function of range from the lidar. The intensity of the return signal also decreases in proportion to the square of the range. The two optical signals are converted to electrical currents in two single-wavelength light detectors, amplified, and converted to voltages that are proportional to the logarithm of the light intensity. The two analog voltages, which are proportional to the logarithm of the received light intensity for each channel, are digitized as pairs of 12 bit data values at a 20 MHz sample rate for a 50 μs duration interval and recorded. The lidar was operated at a 10 Hz pulse repetition rate.

To correct for changing lidar sensitivity versus range, back-scattering signals from atmospheric regions with low aerosol particle concentration were used for sensitivity calibration. Signals from such regions are due to the Rayleigh scattering alone, and therefore exhibit only the range-squared decrease in signal strength and changes in atmospheric molecular density with altitude. Each lidar signal was processed by first selecting a period with only Rayleigh backscatter, averaging this return signal for 15 seconds, then subtracting this time-averaged signal from signals recorded during

other periods in which the aircraft flew over the smoke plume. The differences in signal obtained in this way are equal to the logarithm of the ratio of the optical backscatter from the smoke to the optical backscatter from the smoke-free atmosphere, together with any corrections for changes in lidar sensitivity versus range. This log-ratio signal is then used to determine the ratio of the backscattering from the smoke to Rayleigh backscatter as a function of range. Using the standard value of Rayleigh backscattering at 0.532 μm (Waggoner, *et al.*, 1971), the log-ratio signal can be converted into an optical backscatter due to the smoke. The optical backscatter can be converted to a light-scattering coefficient using measured values of the ratio of lidar optical backscatter to the light-scattering coefficient of particles (Waggoner, *et al.*, 1971). The spatial distribution of smoke was also determined from *in situ* airborne measurements using an integrating nephelometer, which measures the light-scattering coefficient directly.

Figure 5 shows the flight tracks above the plume from the fire on 15 September and Figs. 6–8 show cross sections of the light-scattering coefficient of the smoke plume derived from the downward-pointed lidar measurements, as the aircraft flew 9, 18 and 41 km downwind from the fire. (On 16 September, aircraft sampling was concentrated close to the location of the fire, therefore, no lidar data was obtained in the downwind plume.) Figure 9 shows measurements of the light-scattering coefficient in the plume measured directly with the nephelometer as the aircraft flew transversely through the plume at a downwind distance of 45 km. Note that the measurements of scattering coefficient in figures 6-9 can be converted to particle mass concentration by dividing scattering coefficient by the measured ratio of $\sigma_{scat}/\rho_{part}$ from table 3. On 15 September, the width of the plume between 1 and 1 1/2 hours after ignition at 9 km downwind from the fire was 6 km, at 18 km downwind the plume width was 10 km, and at 41 km downwind the plume width was 11 km.

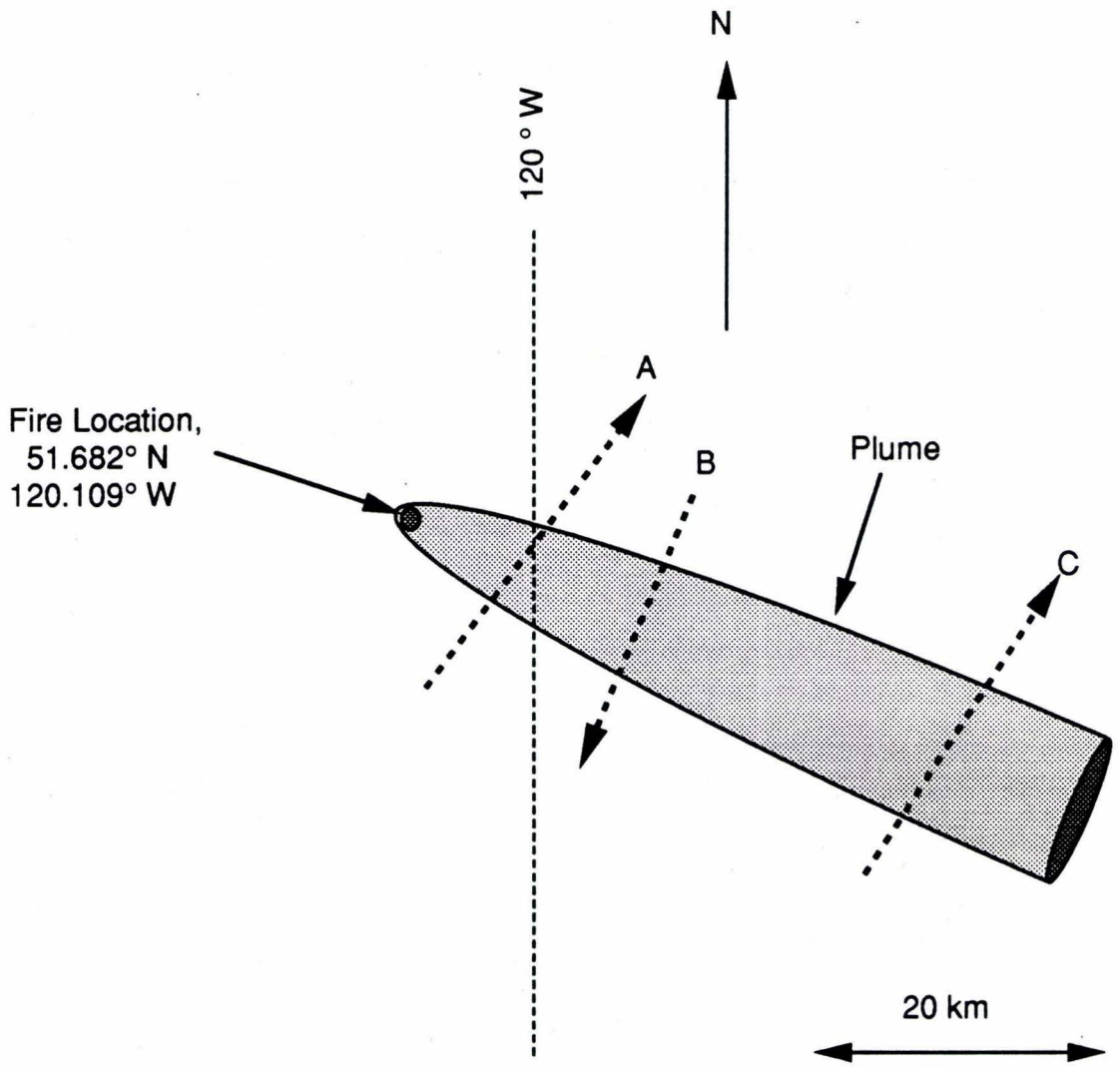

Figure 5. Idealized aircraft flight tracks (dashed lines) over the smoke plume from the prescribed fire on 15 September. Fire ignition was at 14:31 PDT. The approximate plume geometric centerline for path A was crossed over at 15:32:50, path B at 15:36:00, and path C at 15:55:30 PDT. The scattering extinction coefficients in the plume derived from lidar measurements made along these three paths are shown in figures 6 - 8.

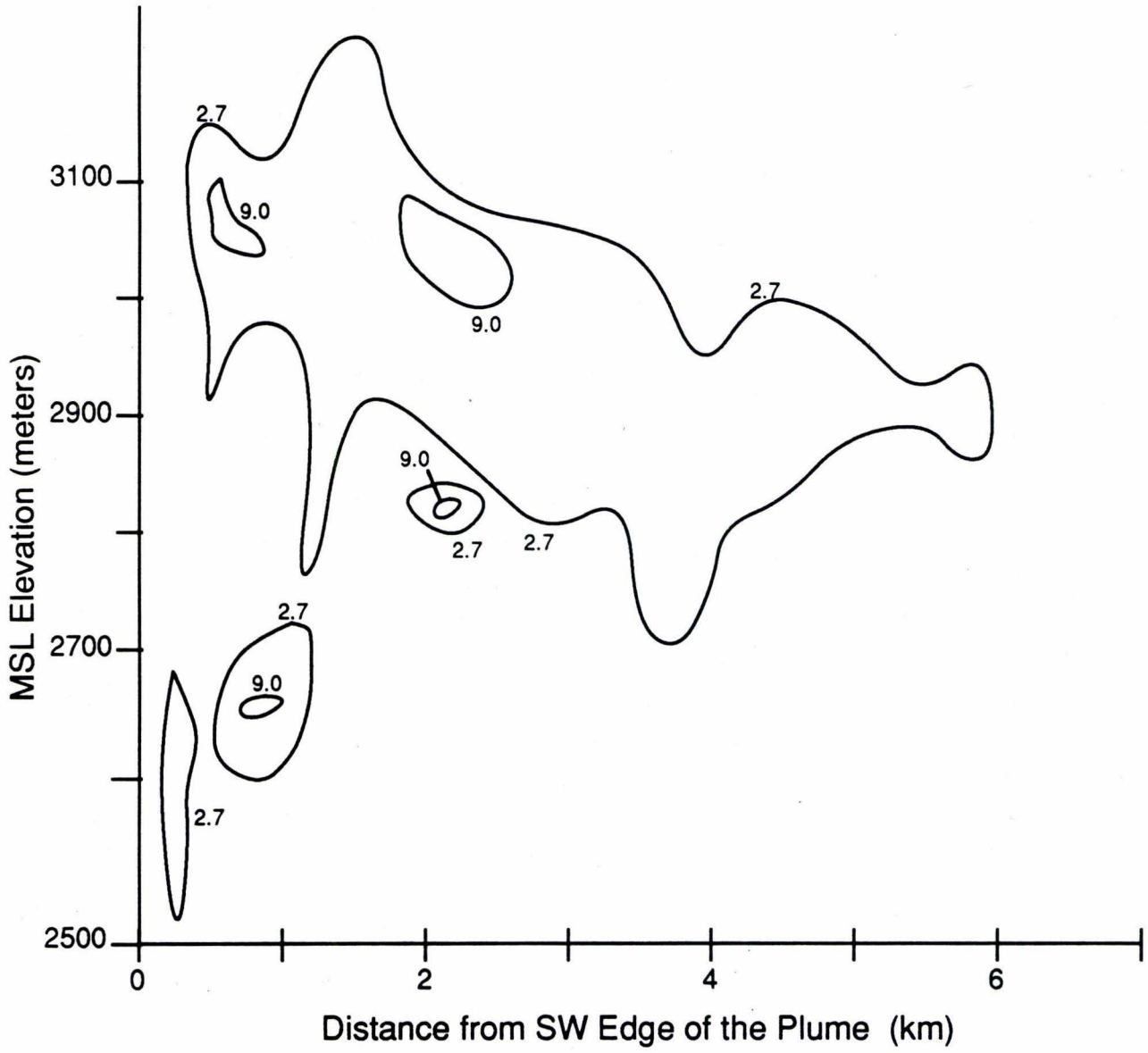

Figure 6. Isopleths of scattering coefficient (at 0.532 μm in units of 10^{-4} m^{-1}), calculated from lidar measurements. This vertical cross-section, through flight path A in Fig. 5, was 9 km downwind from the fire on 15 September 1991, and was obtained 62 minutes after ignition.

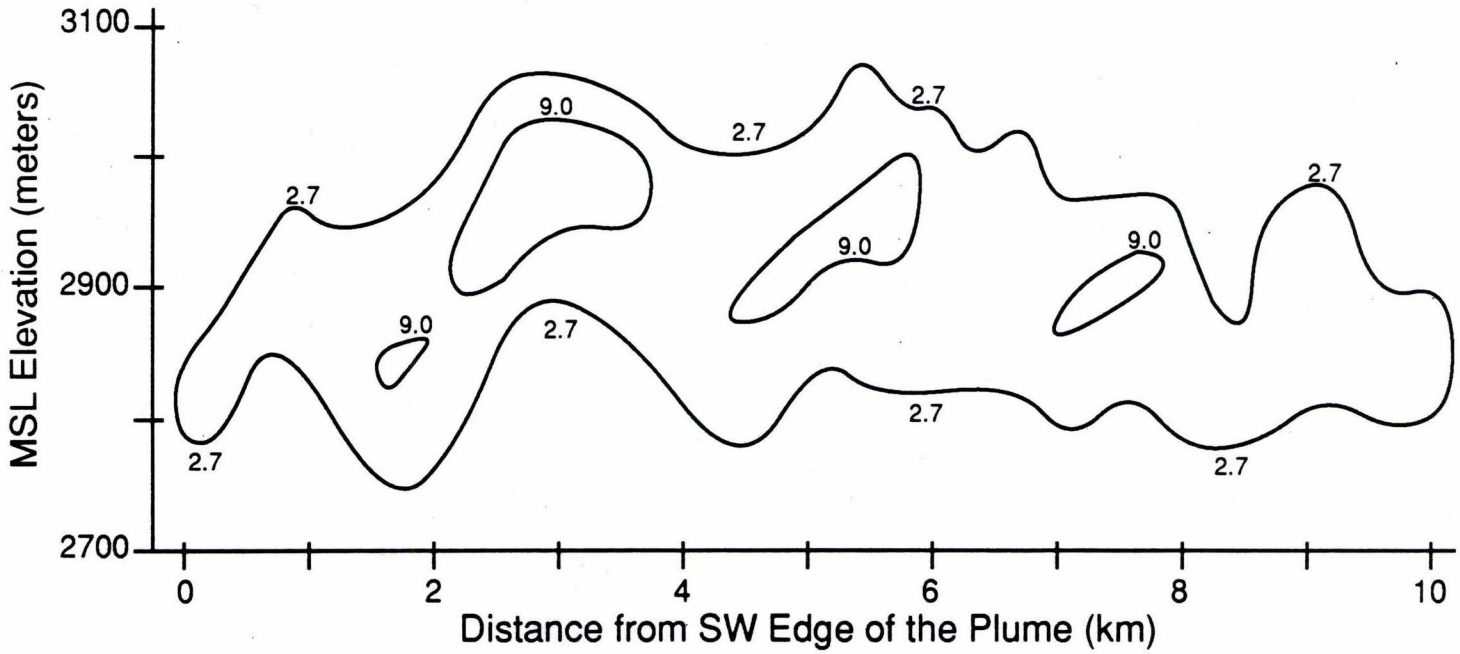

Figure 7. Isopleths of scattering coefficient (at 0.532 μm in units of $10^{-4} m^{-1}$), calculated from lidar measurements. This vertical cross-section, through flight path B in Fig. 5, was 18 km downwind from the fire on 15 September 1991, and was obtained 65 minutes after ignition.

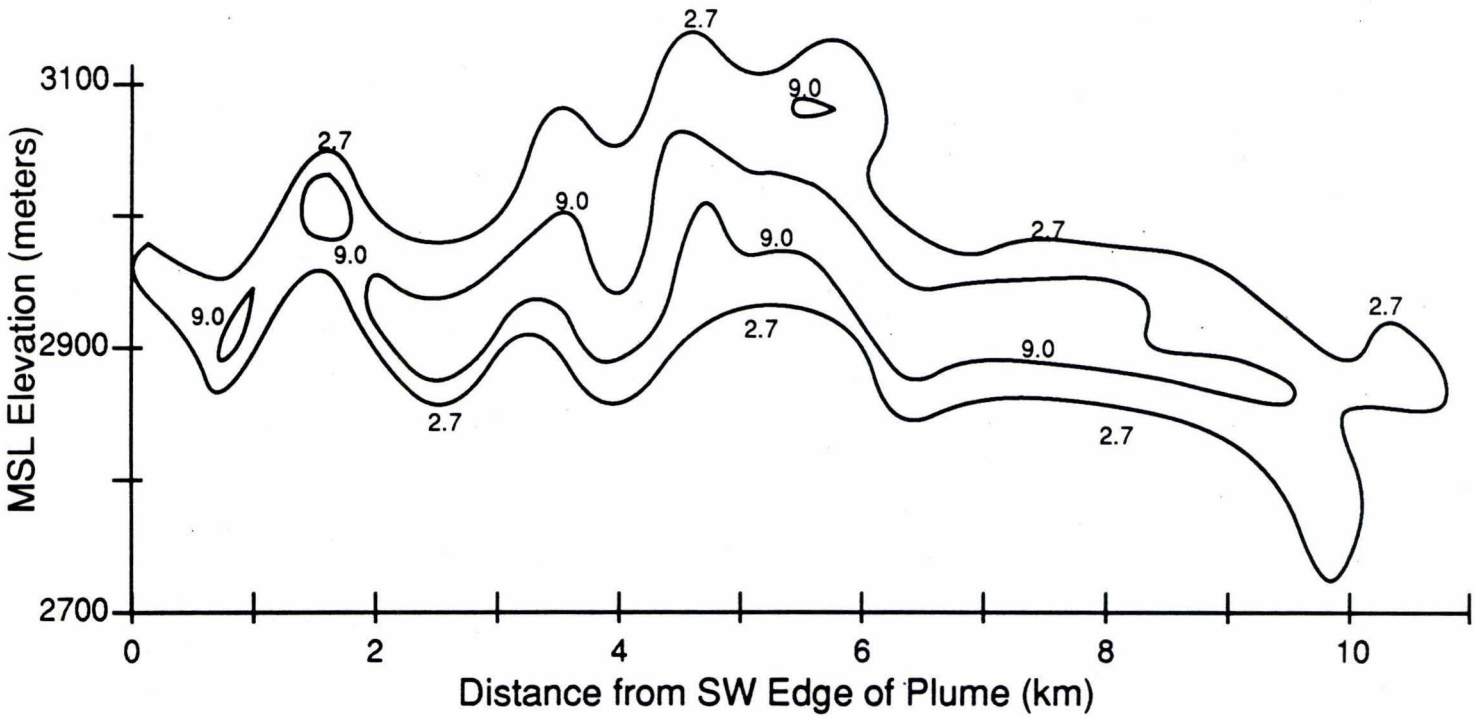

Figure 8. Isopleths of scattering coefficient (at 0.532 μm in units of 10^{-4} m^{-1}), calculated from lidar measurements. This vertical cross-section, through flight path C in Fig. 5, was 41 km downwind from the fire on 15 September 1991, and was obtained 84 minutes after ignition.

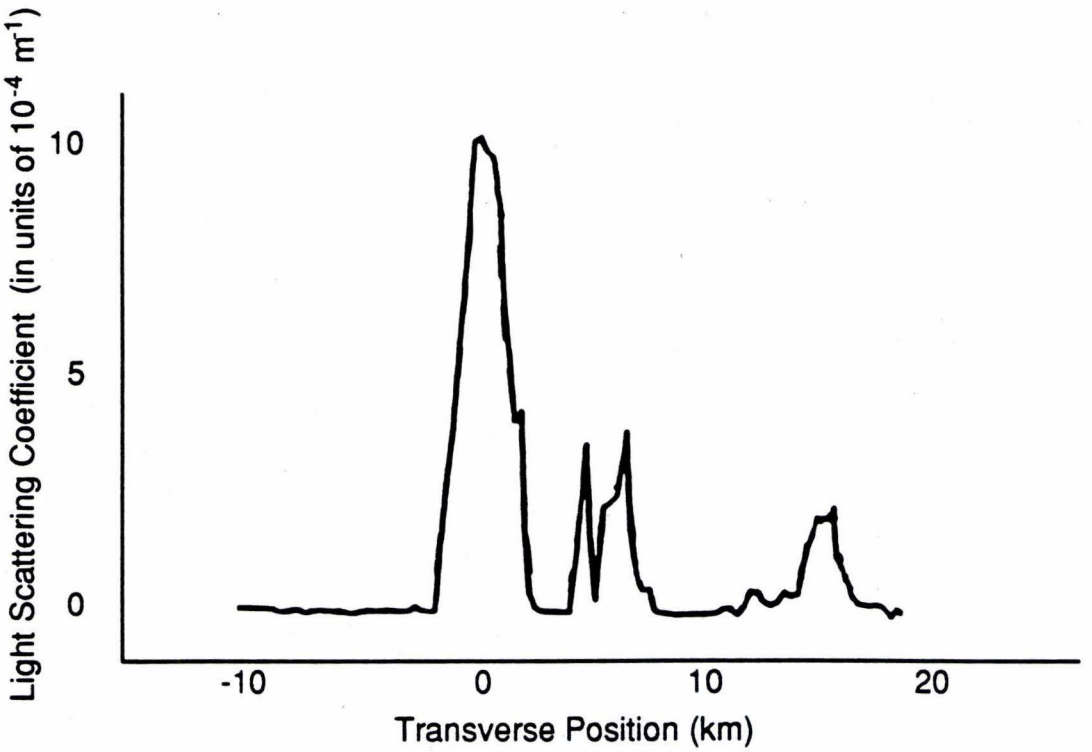

Figure 9. In situ light scattering coefficient at 0.53 μm. The aircraft flew across the width of the plume at an altitude of 2900 meters MSL, 45 km downwind from fire, on 15 September 1991. The center of the plume (indicated by "0" on the absisa) was crossed at 16:07 PDT which was 96 minutes after ignition.

The plume cross sections were complex (e.g. the additional isolated plumes in Fig. 6). The plume stayed at a relatively constant elevation of 2900 meters MSL and did not disperse vertically beyond the original depth of ~300 meters. The cross sections showed much more spatial structure and variations than that described by the Gaussian plume model.

Note that the lidar and nephelometer measurements of the cross-sections of the plume are neither Lagrangian nor simultaneous but are measurements at a series of times, from 62 to 96 minutes after ignition, at down-wind distances of 9 to 45 km from the fire.

4. COMPARISONS WITH SOME OTHER BIOMASS FIRES

Some comparisons between the two fires discussed in this report and other biomass fires studies by the Cloud and Aerosol Research Group are shown in Table 5 and Figs. 10–14. It can be seen that the emissions from the 15 September fire appear anomalous with respect to the other fires. We attribute this to the fact that this fire was sampled only during smoldering combustion. During smoldering combustion, the combustion efficiency is generally lower, the emissions of particles, methane, carbon monoxide and other hydrocarbons higher, and NO_x emission lower, than they are during flaming combustion.

The emission factors for C_2H_2, N_2O and NO_x from the 16 September fire appear elevated compared to the other fires listed in Table 5; this may also reflect sampling conditions. In the 16 September fire, smoke samples were collected during the flaming combustion, when the emissions of NO_x are generally higher (Laursen *et al.*, 1992).

Particle emission factors as a function of time for the 15 and 16 September fires in British Columbia are compared to those for the Mable Lake fire in Eastern British Columbia in Fig. 14. The three fires show similar temporal changes in particle emission factors.

Table 5: Comparison of the average emission factors (and standard deviations) for various trace gases from ten biomass fires in North America with those measured from the two prescribed biomass fires that burned near Clearwater, British Columbia, on 15 and 16 September 1991. All values shown are based on the analyses of samples collected in stainless steel canisters. Units are g kg^{-1}.

Fire	CO_2	CO	CH_4	C_2H_6	C_2H_2	C_3H_8	C_3H_6	N-C_4*	N_2O	NO_x†	Reference
Lodi 1	1664	74	2.4	0.35	0.32	0.21	0.58	0.11	0.31	8.9	Radke et al.
	± 44	± 16	± 0.2	± 0.12	± 0.05	± 0.12	± 0.05	± 0.07	± 0.14	± 3.5	(1991)
Lodi 2	1650	75	3.6	0.55	0.21	0.32	0.46	0.10	0.27	3.3	Radke et al.
	± 31	± 14	± 0.3	± 0.15	± 0.03	± 0.12	± 0.03	± 0.05	± 0.31	± 0.8	(1991)
Myrtle	1626	106	3.0	0.60	0.22	0.25	0.70	0.02		2.5	Radke et al.
	± 39	± 20	± 0.8	± 0.13	± 0.04	± 0.05	± 0.04	± 0.04		± 0.7	(1991)
Silver	1637	89	2.6	0.56	0.19	0.42	0.08	0.20	0.27	0.8	Radke et al.
	± 103	± 50	± 1.6	± 0.33	± 0.09	± 0.13	± 0.01	± 0.10	± 0.39	± 0.7	(1991)
Hardiman	1664	82	1.9	0.45	0.31	0.18	0.58	0.02	0.41	3.3	Radke et al.
	± 62	± 36	± 0.5	± 0.26	± 0.35	± 0.13	± 0.09	± 0.04	± 0.52	± 2.3	(1991)
Eagle	1748	34	0.9	0.18	0.08	0.05	0.25	0.20	0.16	7.2	Radke et al.
	± 11	± 6	± 0.2	± 0.05	± 0.02	± 0.02	± 0.06	± 0.08	± 0.13	± 3.8	(1991)
Battersby	1508	175	5.6	0.57	0.33	0.27	0.90	0.07		1.1	Radke et al.
	± 161	± 91	± 1.7	± 0.45	± 0.06	± 0.12	± 0.15	± 0.06		± 1.3	(1991)
Hill	1646	90	4.2	0.48	0.25	0.15	0.65	0.04	0.18		Radke et al.
	± 50	± 21	± 1.3	± 0.17	± 0.05	± 0.06	± 0.19	± 0.01	± 0.06		(1991)
Wicksteed	1700	55	3.8	0.51	0.22	0.17	0.62	0.04	0.22		Radke et al.
	±82	± 41	± 2.8	± 0.34	± 0.12	± 0.12	± 0.40	± 0.03	± 0.14		(1991)
Mabel Lake	1660	83	3.5	0.38	0.22	0.11	0.46	0.03	0.04		Radke et al.
	± 29	± 37	± 1.9	± 0.21	± 0.06	± 0.07	± 0.21	± 0.01	± 0.05		(1991)
Overall Average	1650	83	3.2	0.46	0.24	0.21	0.53	0.83	0.23	3.9	Radke et al.
Emission Factor	±29	± 16	± 0.5	± 0.08	± 0.04	± 0.05	± 0.08	± 0.28	± 0.05	± 1.6	(1991)
Clearwater 1	1563	112	7.9	1.11	0.61	0.98	0.34	0.08	0.04	0.27	This report
(15 Sept., 1991)	± 32	± 14	± 1.0	± 0.17	± 0.13	± 0.19	± 0.05	± 0.01	± 0.04	± 0.01	
Clearwater 2	1691	58	3.5	0.48	0.59	0.57	0.14	0.05	0.52	0.58	This report
(16 Sept., 1991)	± 28	± 11	± 0.1	± 0.09	± 0.26	± 0.16	± 0.05	± 0.01	± 0.41	± 0.06	

* Normal Butane

† $NO_x = NO + NO_2$

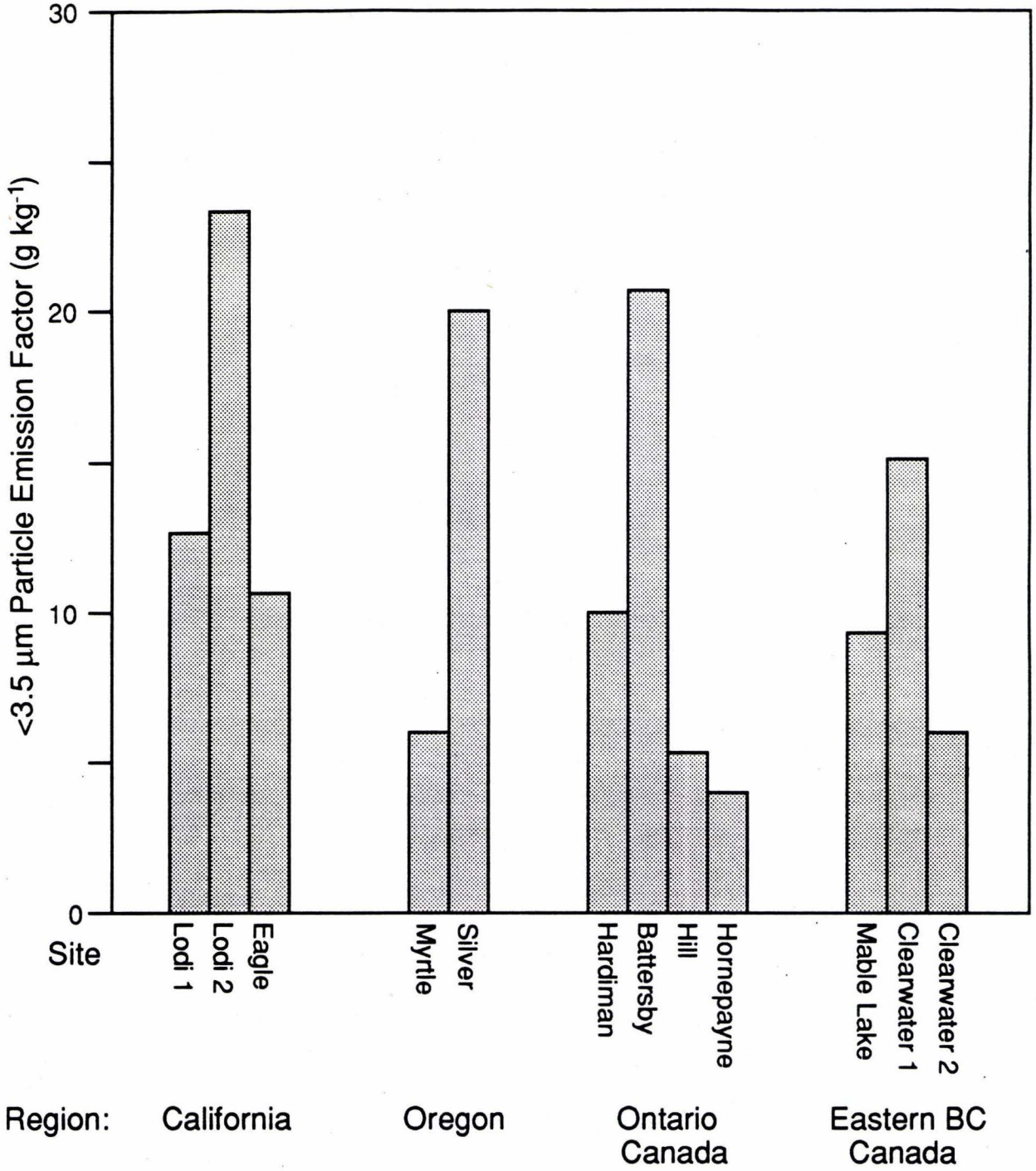

Figure 10. Particle emission factors, grouped by location of fire. The two right-most fires are the subject of this report and were conducted on 15 and 16 September 1991 near Clearwater, British Columbia, Canada. Clearwater 1 contains only data taken later than 45 minutes after ignition of the fire on 15 September.

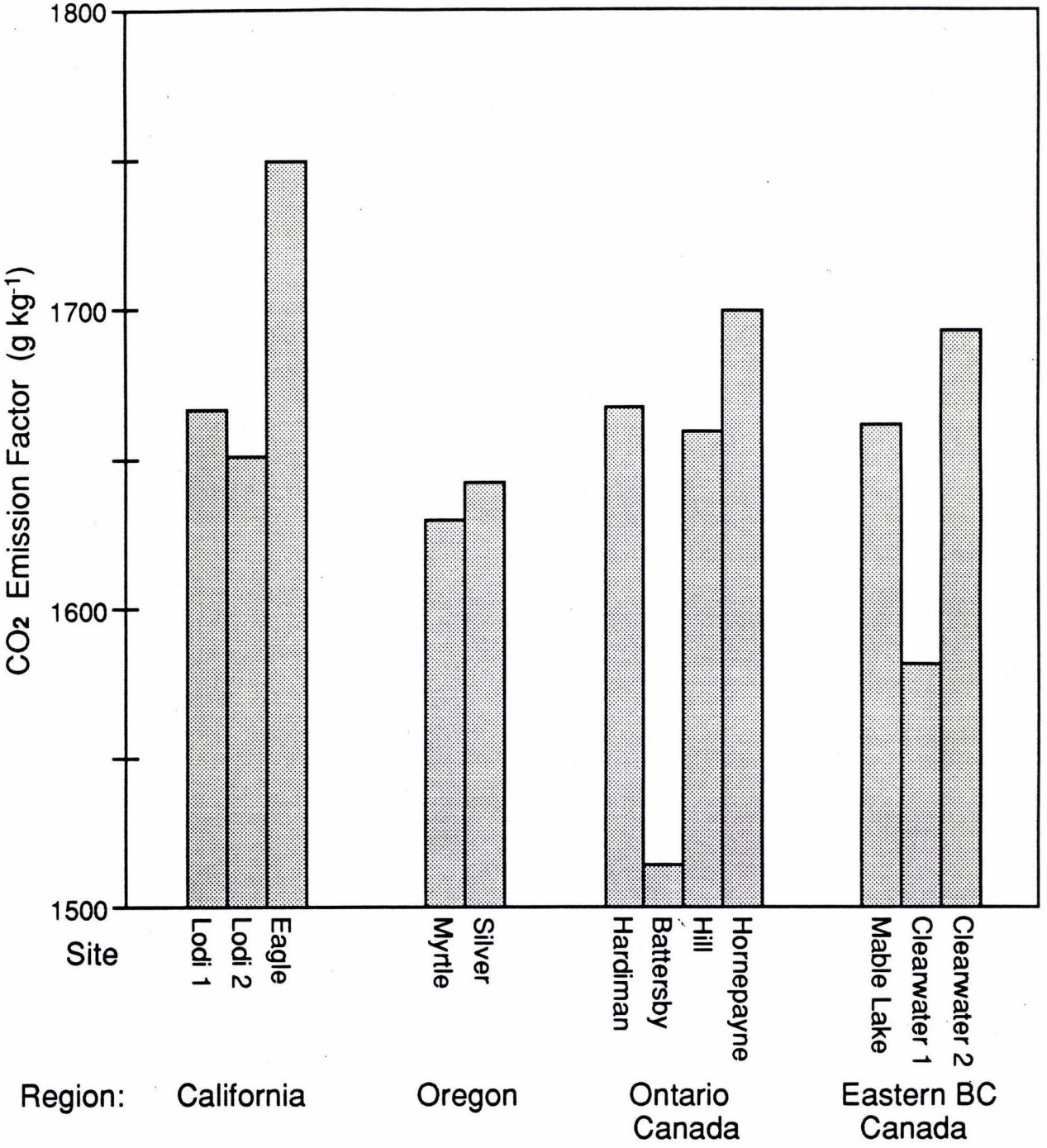

Figure 11. As for Fig. 10 but for carbon dioxide.

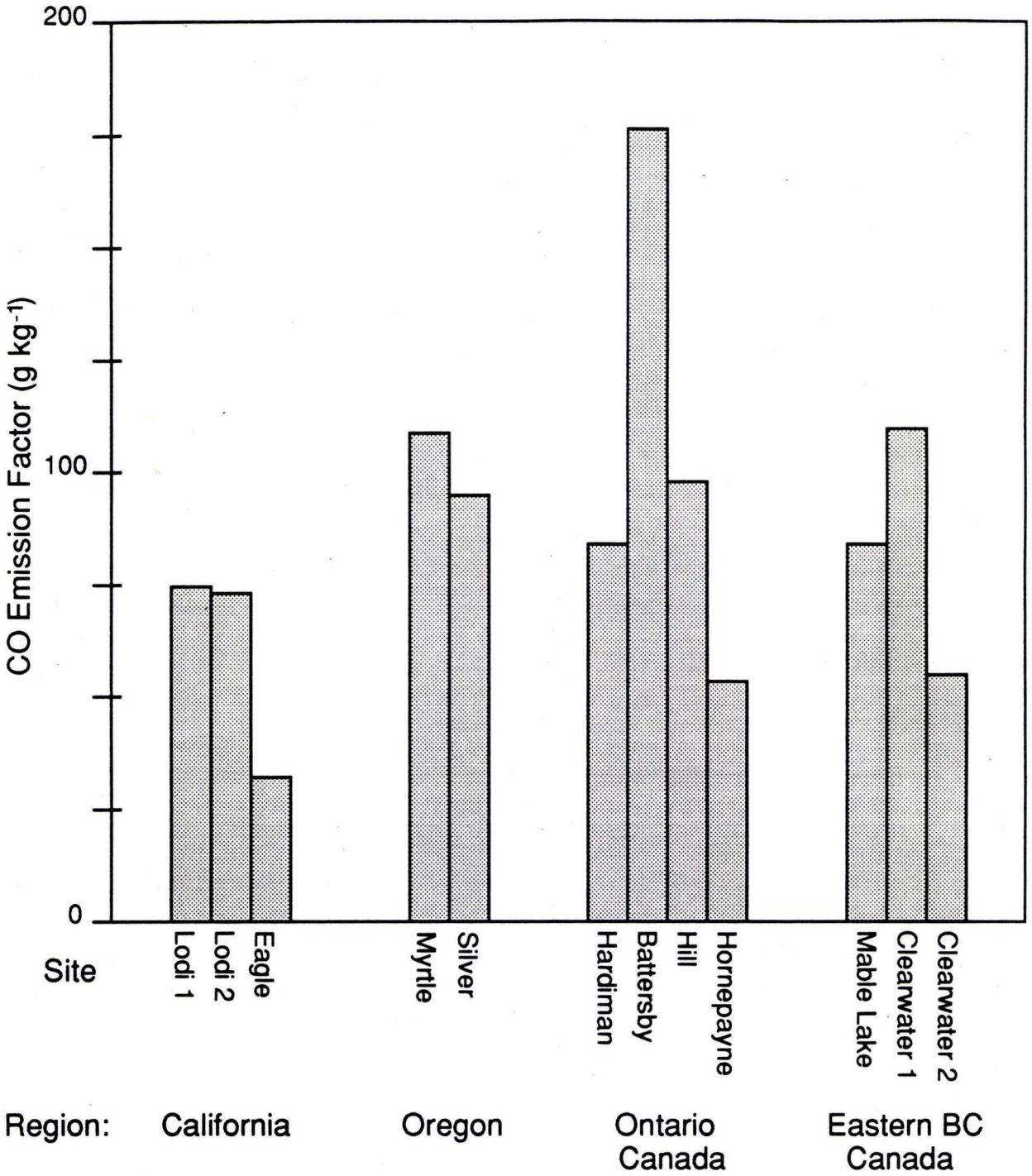

Figure 12. As for Fig. 10 but for carbon monoxide.

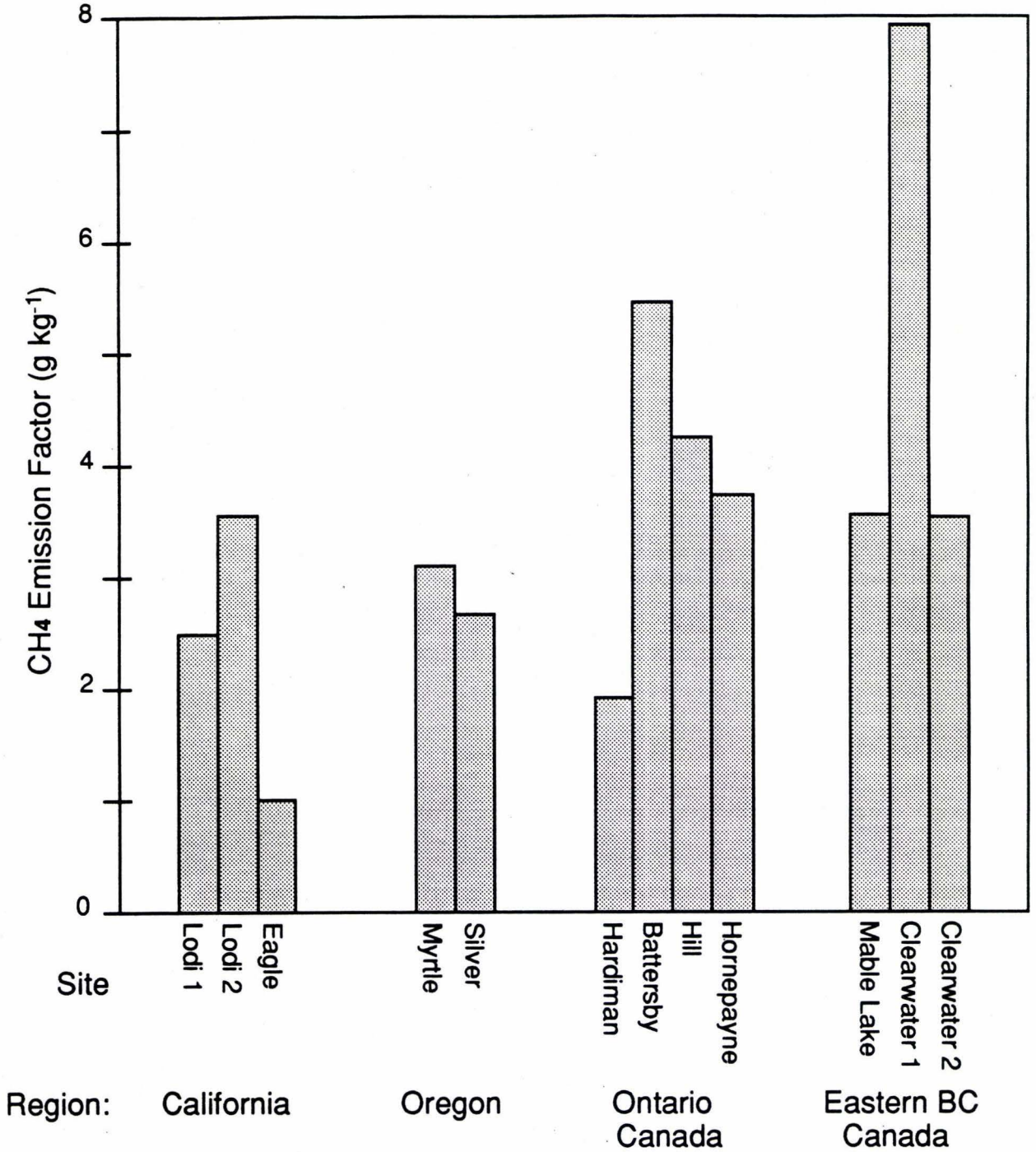

Figure 13. As for Fig. 10 but for methane.

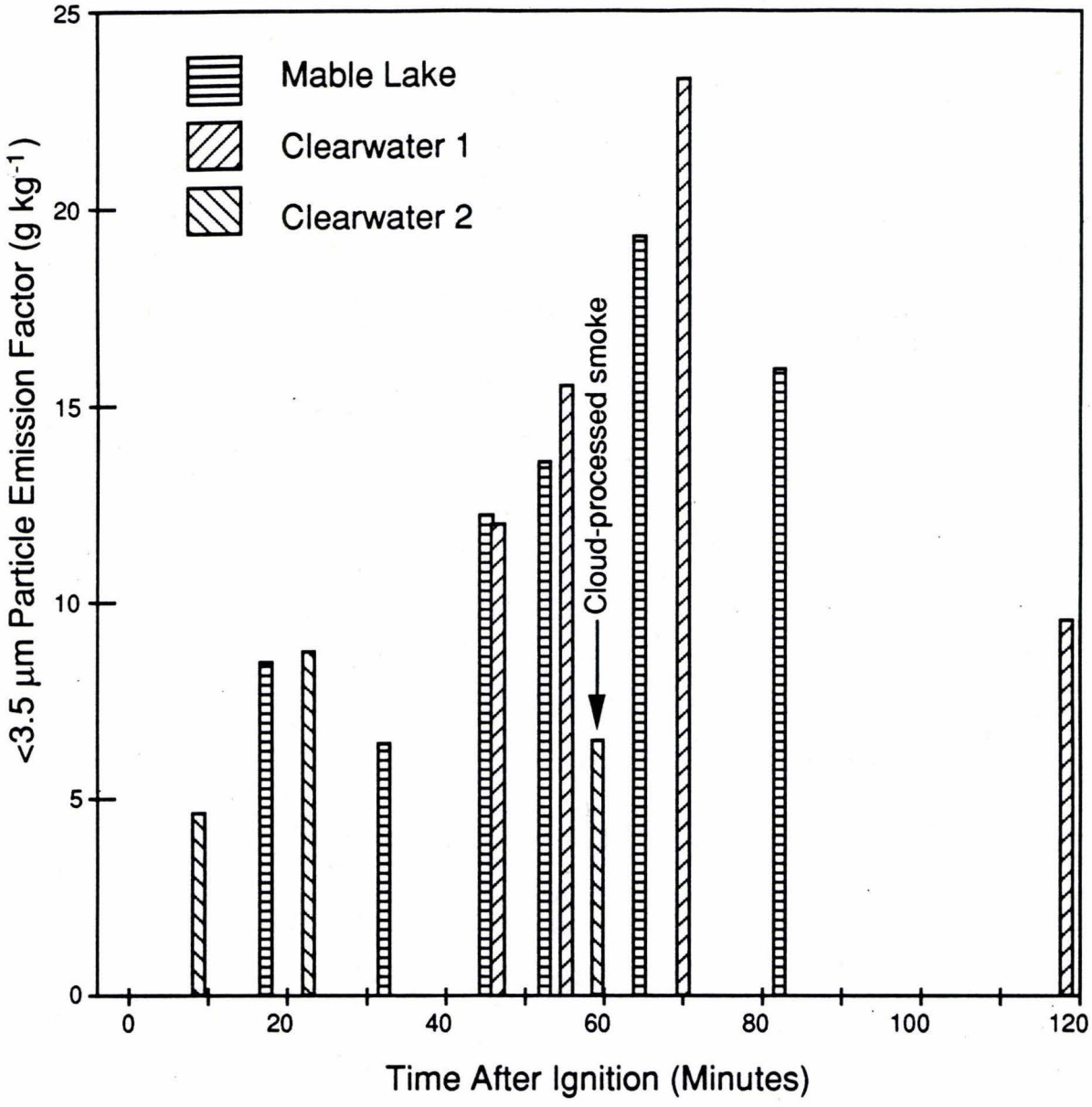

Figure 14. Particle emission factor versus time from ignition. Note the apparently common pattern of increase from ~5 to ~20 g kg^{-1} between 10 and 70 minutes after ignition, followed by a decrease from ~20 to ~10 g kg^{-1} between 70 and 120 minutes after ignition.

5. REFERENCES

Bryam, G. M., Combustion of forest fuels, In Forest Fire Control and Use, K. P. Davis Ed., McGraw-Hill, New York, NY, 1959.

Clements, H. B. and C. K. McMahon, Nitrogen oxides from burning forest fuels examined by thermogravimetry and evolved gas analysis, Thermochimica Acta, 35, 133–139, 1980.

Cofer, W. R., III, J. S. Levine, E. L. Winstead, and B. J. Stocks, Gaseous emissions from Canadian boreal forest fires, Atmos. Environ., 24A, 1653–1659, 1990.

Crutzen, P. J., and M. O. Andreae, Biomass burning in the tropics: impact on atmospheric chemistry and biogeochemical cycles, Science, 250, 1669–1678, 1990.

Evans, L. F., I. A. Weeks, A. J. Eccleston and D. R. Packham, Photochemical ozone in smoke from prescribed burning of forests. Environ. Sci. Tech., 11, 896–900, 1977.

Finlayson-Pitts, B. J. and J. N. Pitts, Jr., Atmospheric Chemistry: Fundamentals and Experimental Techniques, John Wiley & Sons, New York, NY, 1985.

Glassman, I., Combustion, Academic Press, New York, N Y, 1977

Hegg, D. A., L. F. Radke, P. V. Hobbs, C. A. Brock and P. J. Riggan, Nitrogen and sulphur emissions from the burning of forest products near large urban areas, J. Geophys. Res., 92, 14,701–14,709, 1987.

Hobbs, P. V., L. F. Radke, J. H. Lyons, R. J. Ferek, D. J. Coffman and T. J. Casadevall, Airborne measurements of particle and gas emissions from the 1990 volcanic eruptions of Mount Redoubt, J. Geophys. Res., 96, 18,735–18,752, 1991.

Kaputsin, V. N., G. V. Rosenberg, N. C. Ahlquist, D. S. Covert, A. P. Waggoner and R. J. Charlson, Characterization of non-spherical atmospheric aerosol particles with electro-optic nephelometery, Appl. Optics, 19, 1980.

Laursen, K. K., P. V. Hobbs and L. F. Radke, Some trace gas emissions from North American biomass fires with an assessment of regional and global fluxes from biomass burning, J. Geophys. Res, 1992, (in press)

Logan, J. A., Nitrogen oxides in the troposphere: global and regional budgets, J. Geophys. Res., 88, 10,785–10,807, 1983.

Muzio, L. J. and J. C. Kramlich, An artifact in the measurement of N2O from combustion sources, Geophys. Res. Letts., 15, 1369–1372, 1988.

Radke, L. F., D. A. Hegg, P. V. Hobbs, J. D. Nance, J. H. Lyons, K. K. Laursen, R. E. Weiss, P. J. Riggan and D. E. Ward, Particulate and trace gas emissions from large biomass fires in North America. In Global Biomass Burning: Atmospheric, Climate and Biospheric Implications, J. S. Levine Ed., MIT Press, 209–224, 1991.

Radke, L. F., D. A. Hegg, J. H. Lyons, C. A. Brock, P. V. Hobbs, R. E. Weiss and R. A. Rasmussen, Airborne measurements on smokes from biomass burning. In Aerosols and Climate, P. V. Hobbs and M. P. McCormick Eds., A. Deepak Publishing Co., 411–422, 1988.

Rasmssen, R. A. and M. A. K. Khalil, Atmospheric halocarbons: measurements and analyses of selected trace gases, Proceedings of the NATO Advanced Study Institute on Atmospheric Ozone, A. C. Aikin, Ed., U.S. Dept. of Transportation, 1980.

Rasmussen, R. A. and M. A. K. Khalil, Atmospheric methane (CH4): Trends and seasonal cycles, J. Geophys. Res., 86, 9826–9832, 1981.

Susott, R. A., D. A. Ward, R. E. Babbit and D. J. Latham, The measurement of trace emissions and combustion characteristics for a mass fire, In Global Biomass Burning: Atmospheric, Climate and Biospheric Implications, J. S. Levine Ed., MIT Press, 245–257, 1991.

Waggoner, A. P. and R. J. Charlson, Measurements of aerosol optical parameters, in Fine Particles: Aerosol Generation, Measurement, Sampling, and Analysis, B. Y. H. Liu, Ed., Academic Press, New York, 511–533, 1976.

Waggoner, A. P., N. C. Ahlquist and R. J. Charlson, Measurements of the aerosol total scatter-backscatter ratio, Appl. Optics, 11, 2886–2889, 1971.

Waggoner, A. P. and R. E. Weiss, Comparison of fine particle mass concentration and light-scattering extinction in ambient aerosol. Atmos. Environ., 14, 875–876,1980.

Ward, D. E., Factors influencing the emissions of gases and particulate matter from biomass burning, in Fire in the Tropical Biota: Ecosystem Processes and Global Challenges, pp. 418–436, Springer-Verlag, Berlin-Heidelberg, 1990.

Ward, D. E., D. V. Sandberg, R. D. Ottmar, J. A. Anderson, G. C. Hofer, and C. K. Fitzsimmons, Measurements of smokes from two prescribed fires in the Pacific Northwest, Seventy-Fifth Annual Meeting of the Air Pollution Control Association, (Available from D. E. Ward, U.S.D.A. Forest Service, Intermountain Fire Science Laboratory, Missoula, MT 59807), 1982.

Ward, D. E. and Hardy, C. C., Smoke emissions from wildland fires, Environ. Internat., 17, 117–134, 1991.

Weiss, R. E., A. P. Waggoner, R. J. Charlson, D. A. Thorsell, J. S. Hall and L. A. Richy, Studies of the optical, chemical and physical properties of light-absorbing aerosols. In Proceedings of the Conference on Carbonaceous Particles in the Atmosphere, LBL-9037, Conf. #7803101, Berkeley, CA, 257–262, 1979.

Weiss, R. E., V. N. Kapustin and P. V. Hobbs, Chain-aggregate aerosol in smoke from the Kuwait oil fires, J. Geophys. Res., 1992, (in press)

APPENDIX

THE UNIVERSITY OF WASHINGTON'S CONVAIR C-131A RESEARCH AIRCRAFT

All of the airborne measurements needed for this study can be obtained aboard the University of Washington's C-131A aircraft.

General Description of Airborne Facilities

The Convair C-131A is a twin-engine, propeller driven aircraft that is large enough to carry a large instrumentation payload plus a crew of up to eight persons.

The layout of the work stations and major instrumentation units on the aircraft is shown in Figure A.1.

Details on the instrumentation presently aboard the aircraft are given in Table A.1, where they are grouped under the following headings: navigational and flight characteristics, general meteorological, cloud physics, aerosol, cloud and atmospheric chemistry, remote sensing, and data processing and display. The interrelationships between the scientific crew, the various measurement systems, and the data display and recording systems, are shown schematically in Figure A.2.

Data Recording and Data Display

Data from the various instruments aboard the aircraft are digitized and distributed to both a microcomputer for on-board display and an independent digital tape cartridge recording system for post-flight analysis. The flight scientists, systems engineer, cloud and aerosol scientist and atmospheric chemist stations each have terminals and color graphics displays to access data from the computer via a multi-user operating system (see Figure A.2). Software is available to display up to twenty measured parameters, as well as particle and droplet spectra, aircraft position plots, histograms of selected parameters and radar/lidar reflectivity profiles. Fast data-rate instrumentation (such as the lidar, 35 GHz radar and cloud absorption radiometer), employs separate high density magnetic tape recording systems. Time synchronization is assured by the use of a clock signal common to all the measuring systems.

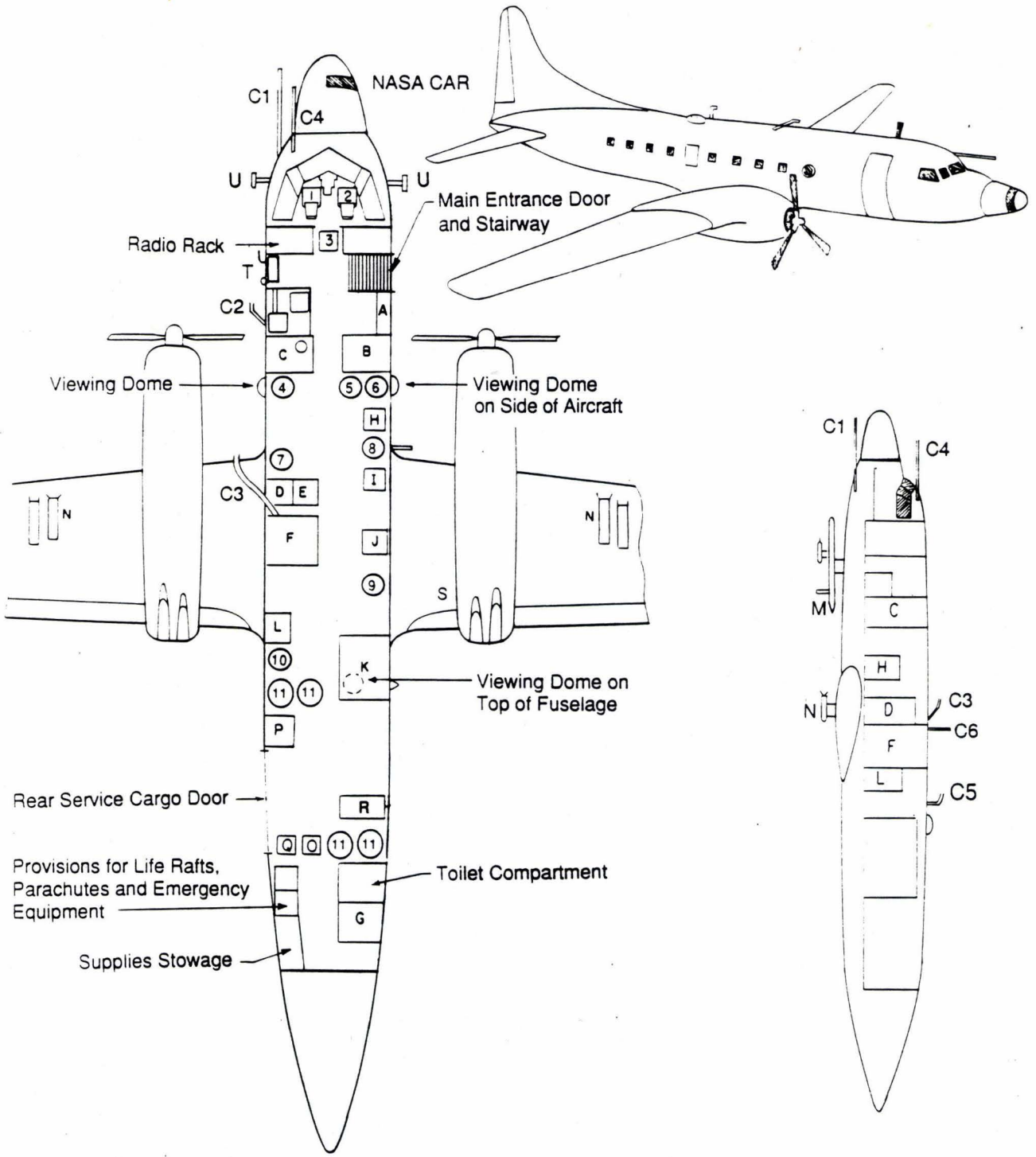

Figure A.1 Layout of work stations and major research instrumentation units aboard the University of Washington's Convair C-131A research aircraft. (See following page for key to letters and numbers.)

KEY TO LETTERS AND NUMBERS IN FIGURE A-1

1. Pilot
2. Co-Pilot
3. Flight Scientist or Meteorologist
4. Aerosol Scientist
5. Flight Scientist or Meteorologist
6. Flight Scientist or Meteorologist
7. Chemist
8. Flight Engineer
9. Cloud Absorption Radiometer (CAR) Operator
10. Cloud Condensation Nucleus (CCN) Counter Operator
11. Take Off and Landing Stations for Science Crew

Locations of Major Research Instrumentation Units

A. Inverters and power distribution.

B. Scientific situation display including digital and graphical monitors, analog and digital hard copies, radio and telecommunications.

C. Primary aerosol characterization system.

- C1. Inlet supplies the grab sampler.
- C2. Inlet supplies the heated plenum and Hi Vol sample ports.
- C3. Inlet supplies the 2.5 m^3 bag sampler and the trace gas detection system.
- C4. Inlet for 7 m long light extinction and light scattering cells.
- C5. Inlet for CVI.
- C6. Inlet for cloud water sampler.

D. Trace gas system for DMS, NO, NO_2, HNO_3, SO_2, O_3, CO and CO_2.

E. Cloud water and wet chemistry system for hydrometeor inorganic and some organic ions, and aqueous H_2O_2.

F. Enclosed 2.5 m^3 bag sampler and aerosol filter system.

G. Vacuum pump cabinet.

H. Data computer and recording system.

I. Controls for meteorological sensors.

J. Cloud absorption radiometer controls and data recorder.

K. Hemispheric viewing dome.

L. Cloud condensation nucleus spectrometer.

M. Pod (located on aircraft belly under position 3) digital weather radar. UW ice particle counter and PMS FSSP probe.

N. Under wing mounts for 1 and 2-D PMS cloud and precipitation probes.

O. Visible, IR and UV net radiometers on the top and bottom of fuselage. Sea surface temperature sensor on bottom of fuselage.

P. Lidar data system and CVI controls.

Q. Nd-YAG Lidar

R. 35 GHz (λ = 0.86 cm) Radar

S. Antennas for 35 GHz radar (upward and downward looking on top and bottom of wing)

T. Ophir IR optical hygrometer

U. Liquid water sensors (J-W and King)

TABLE A.1

TABLE A.1. INSTRUMENTATION ABOARD THE UNIVERSITY OF WASHINGTON'S AIRCRAFT

Parameter	Instrument Type	Manufacturer	Range (and error)
	(a) Navigational and Flight Characteristics		
Latitude and longitude, ground speed and horizontal winds	VLF: Omega navigator	Litton LTN-3000	0 to 300 m s^{-1} (± 1 m s^{-1} groundspeed and ± 1° drift angle)
True airspeed	Variable capacitance	Rosemount Model 831 BA	0 to 250 m s^{-1} (< 0.2%)
Heading	Gyrocompass	King KCS-55A	0 to 360° (± 0.5°)
Pressure altitude	Variable capacitance	Rosemount Model 830 BA	150 to 1100 mb (< 0.2%)
Altitude above terrain	Radar altimeter	AN/APN22	0 to 6 km (< 5%)
Aircraft position and course plotter	Derived from VLF/ OMEGA; GPS	In-house Trimble Nav.	180 km (1 km) Variable
Angle of attack	Potentiometer	Rosemount Model 861	± 23° (< 0.5°)
Rate of climb	Variometer	Ball Engineering	± 12 m s^{-1}
Precipitation and clouds	Scanning weather radar	Bendix King RDS 82 VP	380 km
	(b) General Meteorological		
Total air temperature	Platinum wire resistance	Rosemount Model 102CY2CG + 414 L Bridge	-60 to 40°C (< 0.1°C)
Static air temperature	Reverse-flow thermometer	In-house	-60 to 40°C (< 0.5°C)
Electric field Intensity	Cylindrical field mill	Modified MRI Model 611	0 to 50 kV (< 1 kV)

TABLE A.1. (Continued)

Parameter	Instrument Type	Manufacturer	Range (and error)
	(b) General Meteorological (Continued)		
Dew point	Dew condensation	Cambridge Systems Model TH73-244	-40 to 40°C (< 1°C)
Absolute humidity	IR optical hygrometer	Ophir Corporation Model IR-2000	0 to 10 gm^{-3} (~ 5%)
Air turbulence	Differential	Meteorology Research, Inc. Model 1120	0 to 10 $cm^{2/3}$ s^{-1} (< 10%)
Pyranometer(s) (one downward and one upward viewing)	Eppley thermopile	Eppley Laboratory, Inc. Model PSP	0 to 1400 W m^{-2} (~ 1%)
Sea surface temperature	IR radiometer	Heimann KT-19	variable
Ultraviolet radiation	Barrier-layer photoelectric cell	Eppley Laboratory, Inc. Model 14042	0 - 70 J m^{-2} s^{-1} (< 5%)
Video tape	Forward looking video camera + time code	Sony	VHS format
Video tape	Upward and downward looking video camera	NEC	S-VHS format
	(c) Cloud Physics		
Liquid water content	Hot wire resistance	Johnson-Williams	0 to 2 and 0 to 6 g m^{-3}
Liquid water content	Hot wire resistance	King/PMS	0 to 5 g m^{-3}
Size spectrum cloud particles	Forward lightscattering	Particle Measuring Systems Model FSSP-100	2 to 47 μm*

TABLE A.1. (Continued)

Parameter	Instrument Type	Manufacturer	Range (and error)
	(c) Cloud Physics (Continued)		
Size spectrum of particles	Forward lightscattering	Particle Measuring Systems Model FSSP-300	0.3 to 20 μm
Size spectrum cloud particles	Diode occultation	Particle Measuring Systems Model OAP-200X	20 to 300 μm*
Size spectrum of precipitation particles	Diode occultation	Particle Measuring Systems Model OAP-200Y	300 to 4500 μm*
Images of cloud particles	Diode occultation imaging	Particle Measuring Systems Model OAP-2D-C	Resolution 25 μm*
Images of precipitation particles	Diode imaging	Particle Measuring Systems Model OAP-2D-P	Resolution 200 μm*
Ice particle concentrations	Optical polarization technique	In-house	0 to 1000 l-1 detects particles (> 50 μm)*
	(d) Aerosol		
Number concentrations of particles	Light transmission	General Electric Model CNC II	10^2 to 10^6 cm^{-3} (particles > 0.005 μm)*
Cloud condensation nucleus spectrometer	Vertical-plate continuous flow	In-house	4 selectable supersaturations between 0.2 and 2%.
Mass concentration particles	Electrostatic deposition onto matched oscillators	Thermal Systems, Inc. Model 3205	0.1 to 3000 μg m^{-3} (< 0.2 μg m^{-3})
Size spectrum of particles	Electric aerosol analyzer	Thermal Systems, Inc. Model 3030	0.0032 to 1.0 μm*

* All particle sizes refer to maximum particle dimensions

TABLE A.1. (Continued)

Parameter	Instrument Type	Manufacturer	Range (and error)
	(d) Aerosol (Continued)		
Size spectrum of particles	90° lightscattering	Particle Measuring System (LAS-200)	0.5 to 11 μm*
Size spectrum of particles	Electrical mobility analyzer	Thermal Systems Inc. DMPS	0.01 to 0.6 μm
Size spectrum of particles	Forward lightscattering	Royco 245 (In-house modified)	1.5 to 40 μm*
Size spectrum of particles	Diffusion battery	Thermal Systems, Inc. Model 3040 with in-house automatic valves and sequencing	0.01 to 0.2 μm*
Size spectrum of particles	35 - 120° lightscattering	Particle Measuring Systems Model ASASP-X	0.09 to 3.0 μm (< 0.007 μm)*
Size spectrum of particles	Forward lightscattering	Particle Measuring Systems Model FSSP-100X	2 to 47 μm*
Size spectrum of particles	Forward lightscattering	Particle Measuring Systems Model FSSP-300	0.3 to 20 μm
Size-segregated concentrations of particles	Cascade impactor	Sierra Instruments Inc.	0.1 to 3 μm* (6 size fractions)
Light-scattering coefficient	Integrating nephelometer	Meteorology Research, Inc. Model 1567 (modified for increased stability and better response time)	1.0×10^{-6} m^{-1} to 2.5×10^{-3} m^{-1}
Light-extinction coefficient	Optical extinction cell (7 m path length)	Waggoner Electronics	5×10^{-5} to 10^{-2} m^{-1}

* All particle sizes refer to maximum particle dimensions

TABLE A.1. (Continued)

Parameter	Instrument Type	Manufacturer	Range (and error)
	(e) Cloud and Atmospheric Chemistry		
Cloud water samples	Impaction on slotted rods	In-house modification of ASRC sampler	Bulk cloud water collection efficiency ~ 40% based on analysis of in-house flight data
Cloud droplet nucleus collector	Counterflow virtual impactor	In-house	Drops > 7 μm diameter
Particulate sulfur $SO_4^=$, NO_3^-, Cl^-, Na^+, K^+, NH_4^+,	Teflon filters CSI & XRF spectroscopy and Dionex ion exchange chromatography	In-house	0.1 to 50 μg m^{-3} (for 500 liter air sample)
SO_2	Impregnated filters	In-house	≥ 9 (±6) pptv (for 4 m^3 air sample)
SO_2	Pulsed fluorescence	Teco 43S	0.1 ppb to 200 ppb
SO_2	Pulsed fluorescence	Teco 43 (modified in-house)	1 ppb to 1 ppm
Ozone	Chemiluminescence (C_2H_4)	Monitor Labs Model 8410 A	0 to 5 ppm (< 7 ppb)
NO, NO_2, NO_x	Chemiluminescence (O_3)	Modified Monitor Labs Model 8840	0 to 5 ppm (~ 0.5 ppb)
HNO_3	Nylon filters with teflon pre-filter followed by ion chromatography and/or tungstic acid denuder tubes followed by chemiluminescent detection	Dionex/Monitor Labs	Variable
CO	Correlation spectrometer	Teco Model 48	0 - 50 ppm (~ 0.1 ppm)
CO_2	Correlation spectrometer	Customized Teco Model 41H	0 - 1000 ppm (~ 4 ppm)
DMS	Absorption on gold wire, followed by gas chromatography with flame photometric detection	In-house	> 1 pptv (± 10%)

TABLE A.1. (Continued)

Parameter	Instrument Type	Manufacturer	Range (and error)
	(f) Remote Sensing		
Absorption and scattering of solar radiation by clouds and aerosols	Scanning cloud absorption radiometer	NASA-Goddard/ U of Washington	13 wavelengths between 0.5 and and 2.3 μm
Radar reflectivity	Pulsed 35 GHz (λ = 0.86 cm) radar	In-house	Upward and downward pointing (600 m to 20 km)
Optical backscatter	Nd-YAG lidar (dual-wavelength, polarization diversity)	Georgia Tech & U. of Wash.	0-15 km (7.5 m resolution)
Precipitation and clouds	Scanning weather radar	Bendix King RDS 82 VP	380 km
	(g) Data Processing and Display		
Ground communication	FM transceiver	Motorola	200 km
In-flight data processing	Microcomputer	In-house, based on Motorola MVME-133A technology	--
In flight color graphics	Microcomputer	In-House, based on Motorola MVME-133A technology	--
Recording (digital)	Microcomputer-directed cartridge recorder	In-house, based on 3M technology	--
Recording (digital)	Floppy disk	---	--
Recording (analog voice transcription)	Cassette recorder	Radio Shack	--
Digital printout	Impact printer	Epson MX-80	
Analog strip charts ink recorder	8-channel high-speed	Soltec T200-839	--

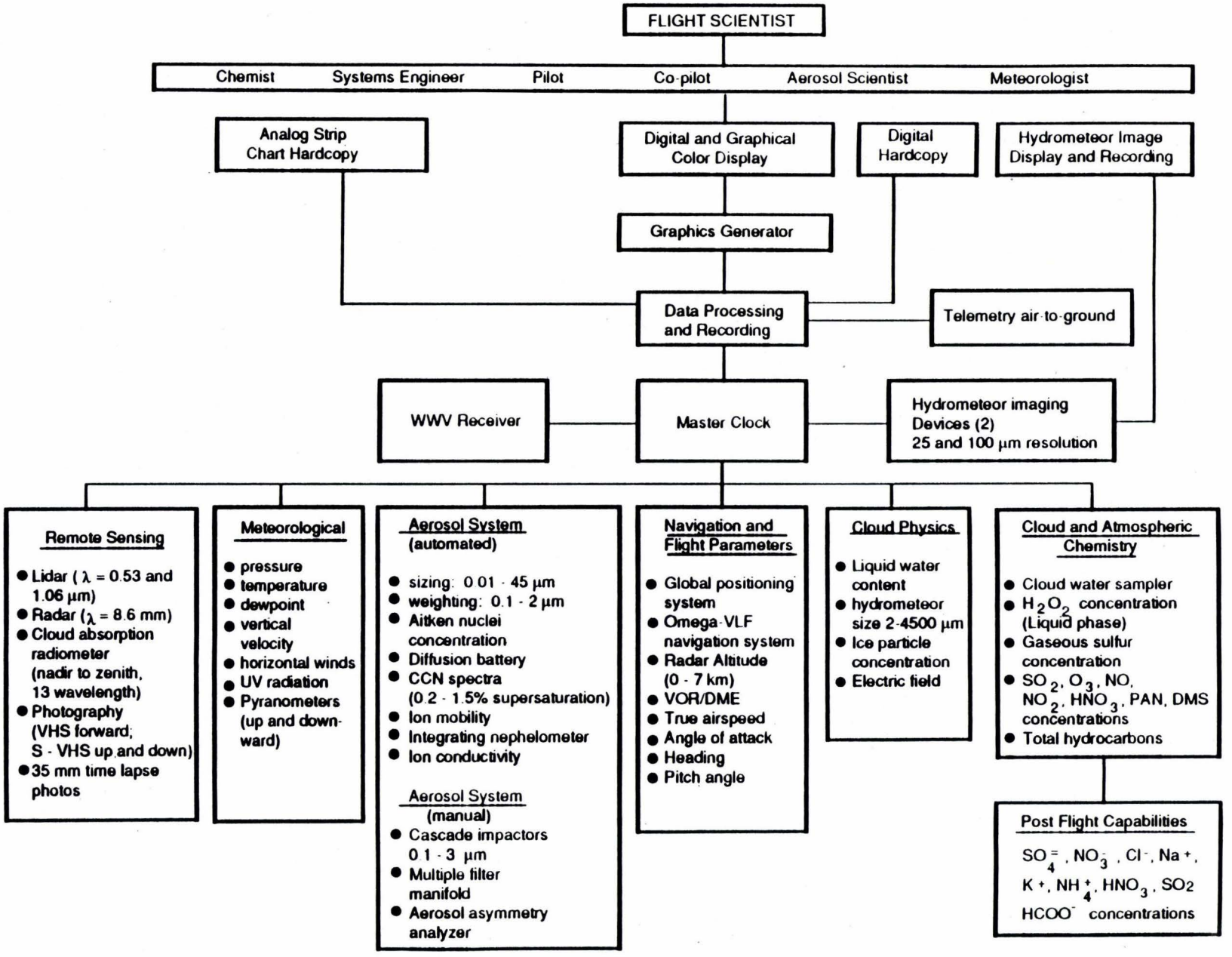

Figure A.2. Scientific crew, measuring systems and data display and recording systems aboard the University of Washington's Convair C-131A research aircraft.